OXFORD

human reproduction

Human Reproduction, 2025, **00(00)**, 1–17
https://doi.org/10.1093/humrep/deaf116
Original Article

Embryology

Paracetamol (N-acetyl-para-aminophenol) disrupts early embryogenesis by cell cycle inhibition

Brian S. Nielsen[1,2,†], Morten R. Petersen[3,†], Javier Martin-Gonzalez[4], Christian Holmberg[5], Heidi K. Mjoseng[1,2,6], Hanne Frederiksen[1], Cristal Rosenthal[5], Emma M. Jørgensen[5], Palle Serup[6,‡], Sarah L. Christensen[7,8,9], Kathrine B. Petersen[8], Karsten Kristiansen[5], Niklas R. Jørgensen[8,10], Jeppe Kari[2], Anders Hay-Schmidt[11], Margaux Heurte[12], Per A. Pedersen[5], Anders Juul[1,8], Anja Pinborg[3], Søren Ziebe[3], Svend Lindenberg[13], Jimmi Elers[14], Arthur David[12], Frederikke Lindenberg[13], Anne Zedeler[15], Søren T. Christensen[5], David M. Kristensen[1,2,12,*]

[1]Department of Growth and Reproduction, Copenhagen University Hospital—Rigshospitalet, Copenhagen, Denmark
[2]Department of Science and Environment, Roskilde University, Roskilde, Denmark
[3]The Fertility Department, Copenhagen University Hospital—Rigshospitalet, Copenhagen, Denmark
[4]Core Facility for Transgenic Mice, Department of Experimental Medicine, University of Copenhagen, Copenhagen, Denmark
[5]Department of Biology, University of Copenhagen, Copenhagen, Denmark
[6]Novo Nordisk Foundation Center for Stem Cell Medicine (reNEW), University of Copenhagen, Copenhagen, Denmark
[7]Department of Neurology, Danish Headache Center, Copenhagen University Hospital—Rigshospitalet, Copenhagen, Denmark
[8]Department of Clinical Medicine, University of Copenhagen, Copenhagen, Denmark
[9]Department of Anesthesia, Critical Care and Pain Medicine, Beth Israel Deaconess Medical Center, Harvard Medical School, Boston, USA
[10]Department of Clinical Biochemistry, Copenhagen University Hospital—Rigshospitalet, Copenhagen, Denmark
[11]Department of Odontology, Faculty of Health, University of Copenhagen, Copenhagen, Denmark
[12]Univ Rennes, Inserm, EHESP, Irset (Institut de recherche en santé, environnement et travail)—UMR_S 1085, Rennes, France
[13]Copenhagen Fertility Center, Section for Research, Copenhagen, Denmark
[14]Stork & DanFert Fertility Clinic, Copenhagen, Denmark
[15]Department of Obstetrics and Gynaecology, The Fertility Clinic, Copenhagen University Hospital, Hvidovre, Denmark

*Correspondence address. Department of Growth and Reproduction, Copenhagen University Hospital—Rigshospitalet, Blegdamsvej 9, DK-2100 Copenhagen, Denmark; Department of Science and Environment, Roskilde University, Universitetsvej 1, DK-4000 Roskilde, Denmark. Tel: +45-5091-5988.
E-mail: david.moebjerg.boslev.kristensen@regionh.dk https://orcid.org/0000-0003-0657-1632

†These authors contributed equally to this work.

‡Author deceased.

ABSTRACT

STUDY QUESTION: Does paracetamol (N-acetyl-para-aminophenol (APAP) also known as acetaminophen) interfere with cell division and thereby disrupt pre-implantation embryonic development?

SUMMARY ANSWER: Our findings suggest that APAP exposure inhibits cell cycling during pre-implantation development (PID) through the reduction of DNA synthesis, potentially resulting in early embryonic loss.

WHAT IS KNOWN ALREADY: It is estimated that 10–40% of all human conceptions fail around the time of implantation. Genetic factors explain ∼50% of early embryonic loss, leaving a substantial portion of early losses without a known cause. Smoking and alcohol are established risk factors for spontaneous abortion, underscoring the importance of the chemical environment during embryonic development.

STUDY DESIGN, SIZE, DURATION: To address the challenges in determining the mechanism of action and the effects of APAP during PID, we utilized a range of approaches, including *in vitro*, *ex vivo*, and *in vivo* methods across various models ranging from yeasts to human embryos and women of fertile age.

PARTICIPANTS/MATERIALS, SETTING, METHODS: A total of 90 human embryos were exposed *in vitro* (22 cleavage stage and 68 blastocyst-stage embryos). Endometrial tissue and uterine fluid were collected from seven women as part of an endometrial scratching procedure. Follicular fluid was collected from 26 women during transvaginal ultrasound guided aspiration of the pre-ovulatory follicles. All human material was sampled in accordance with relevant guidelines and regulations with consent from the regional scientific ethical committee of the Capital Region of Denmark and signed informed patient consent given prior to donation. All mouse experiments were approved by the Danish Animal Experiments Inspectorate and under EU directive 2010/63/EU on the protection of animals used for scientific purposes. The cultivation of the human embryonic stem cell lines H1 and HUES4 was conducted in compliance with relevant guidelines and regulations, following approval from the regional scientific ethical committee of the Capital Region of Denmark.

MAIN RESULTS AND THE ROLE OF CHANCE: After exposure to APAP, we found an unequivocal repression of cell division across all used model systems. APAP exposure hindered cell cycle progression, likely by inhibiting ribonucleotide reductase, leading to reduced DNA synthesis and accumulation in the S-phase. At concentrations found in the reproductive system of women after standard dosing, APAP exposure decreased cell numbers in mouse and human cleavage-stage embryos or caused direct embryonic death.

Received: January 31, 2025. **Revised:** May 7, 2025. **Editorial decision:** May 28, 2025.

Similar exposure to mouse and human blastocyst-stage embryos resulted in a reduced inner cell mass and decreased DNA synthesis, respectively.

LIMITATIONS, REASONS FOR CAUTION: A limitation of the study is the low number of available human cleavage-stage embryos. However, the high number of human blastocysts and our translational approach, which demonstrated reproducibility across various model systems, partly addressed this limitation. Further studies are needed to confirm the potential association between APAP use and pregnancy loss in prospective cohorts.

WIDER IMPLICATIONS OF THE FINDINGS: Our findings indicate that the widely used mild analgesic APAP could contribute to early embryonic loss by impairing initial cell divisions. These results suggest that APAP should be used with caution by women attempting to conceive. Given that cell division is fundamental to all development, further investigation is now warranted to substantiate these findings and to elucidate possible implications for other developmental processes, such as gonadal and brain differentiation.

STUDY FUNDING/COMPETING INTEREST(S): The research was funded by the Lundbeck Foundation (R324-2019-1881). Authors P.S. and H.K.M. were affiliated with the Novo Nordisk Foundation Center for Stem Cell Medicine (reNEW; NNF21CC0073729). H.K.M. received a fellowship from the Novo Nordisk Foundation as part of the Copenhagen Bioscience PhD Program, supported by grant NNF19SA003544. M.H and A.D. are part of the National French Research Infrastructure France Exposome and have received funding from the European Regional Development Fund and Britanny region (Contrat Plan Etat Region, project Exposome, AIDEN 106201).

TRIAL REGISTRATION NUMBER: N/A.

Keywords: paracetamol / acetaminophen / cell cycle / DNA synthesis inhibition / ribonucleotide reductase / early embryo development / embryonic loss

Introduction

A considerable percentage of human conceptions are lost before birth (Roberts and Lowe, 1975; Wilcox *et al.*, 1988). Data from the last decades have shown that an estimated 10–40% of all embryos fail to implant, and an additional 10% of pregnancies are likely lost after implantation but before clinical recognition (Roberts and Lowe, 1975; Wilcox *et al.*, 1988, 1999; Zinaman *et al.*, 1996; Wang *et al.*, 2003; Jarvis, 2016a,b; Foo *et al.*, 2020; Muter *et al.*, 2023). Pre-implantation genetic studies have indicated that chromosomal abnormalities as aneuploidy contribute to ∼50% of peri-implantation loss (Yang *et al.*, 2012; Iwasa *et al.*, 2023), indicating that environmental factors play a role in the loss of early pregnancies (Regan and Rai, 2000; Brown, 2008). Established risk factors, such as smoking and alcohol consumption, further underscore the significance of the chemical environment during early development (Regan and Rai, 2000). Recent studies have also shown that the vaginal microbiota play a role during development, especially among certain ethnic groups (Callahan *et al.*, 2017; Elovitz *et al.*, 2019; Fettweis *et al.*, 2019; Serrano *et al.*, 2019). While these studies have yielded novel insights into abortion and preterm labor, they do not fully elucidate the risk of early embryonic loss within the first weeks of pregnancy.

Over-the-counter mild analgesic paracetamol (N-acetyl-para-aminophenol (APAP), otherwise known as acetaminophen) is the active pharmaceutical ingredient in more than 600 different medications used to relieve mild to moderate pain and reduce fever (Bauer *et al.*, 2021). APAP is widely used by women of reproductive age and during pregnancy, as the compound has been considered of minimal risk for use during pregnancy, when used as directed (Food and Drug Administration, 2015; Kristensen *et al.*, 2016; European Medicines Agency, 2019). Although studies have shown that APAP exposure at non-cytotoxic levels inhibits cell proliferation, impairs DNA repair, and increases DNA fragmentation (Hongslo *et al.*, 1990; Brunborg *et al.*, 1995; Wiger *et al.*, 1997; Holm *et al.*, 2016; Smarr *et al.*, 2017), up to 65% of pregnant women in the USA and an estimated 50% globally use APAP (Werler *et al.*, 2005; Servey and Chang, 2014; Masarwa *et al.*, 2018; Bertoldi *et al.*, 2020). Moreover, APAP is a frequent pollutant of the world's rivers and waterways (Wilkinson *et al.*, 2022), and ubiquitous environmental background exposure to APAP has been found in several European countries (Modick *et al.*, 2014; Nielsen *et al.*, 2015; Bornehag *et al.*, 2018).

We investigated whether APAP interferes with cell division and pre-implantation development (PID). To address the challenges in determining the mechanism of action and the effects of APAP during PID, we utilized a range of approaches, including *in vitro*, *ex vivo*, and *in vivo* methods across model organisms and humans, spanning from yeasts to human embryos and women of fertile age. Our results show that APAP restricts cell proliferation via inhibition of DNA synthesis and that exposure during PID might disrupt development.

Materials and methods

Fission yeast culture

For growth assessment on solid agar, fission yeast (*Schizosaccharomyces pombe*) strains of indicated genotypes were grown overnight in yeast extract liquid medium. Cells were then counted, and diluted to 5000, 500, 50, and 5 cells/µl. Five microliters of each dilution were spotted onto rich medium agar plates containing 1% (v/v) dimethyl sulfoxide (DMSO) or 1% (v/v) DMSO/APAP and incubated for 3 days at 32°C before photography. The growth assessment spot tests were performed as three independent experiments. For growth assessment in liquid yeast extract, fission yeast strains of indicated genotypes were grown at 32°C in the presence of 1% (v/v) DMSO or 40 mM APAP/1% (v/v) DMSO and were monitored by triplicate cell counting using a NucleoCounter® NC-3000™ (ChemoMetec, Lillerød, Denmark) as described by the manufacturer. Doubling time was calculated assuming exponential growth. Samples for DNA content were fixed in 70% (v/v) ethanol, washed in 20 mM EDTA, and treated with RNAse A overnight before staining of the DNA with CytoxGreen and analysis of cellular DNA content using the NucleoCounter® NC-3000™ (ChemoMetec, Lillerød, Denmark) as described by the manufacturer.

Molecular docking

Docking was done using a machine learning-based molecular docking software DiffDock (Corso *et al.*, 2022) to investigate the binding interactions of APAP with the β-RNR from *S. pombe* (UniProt ID: P36603). The structure of the β subunit was predicted *in silico* using AlphaFold3 including iron atoms as cofactors. The structure was solved *in silico* using AlphaFold3 (Abramson *et al.*, 2024) including iron atoms as cofactors. The DiffDock algorithm utilized its diffusion model and score-based generative approach to predict the optimal binding pose. The ligand with the lowest

conformational energy (indicating the highest affinity), as judged by the smina minimized affinity score, was chosen as the most stable binding pose of APAP. The protein–ligand binding interactions were visualized in 2D interaction diagram using PoseView (Stierand *et al.*, 2006).

Human cell culture

Cell culture

HEK293 cells were cultured in high glucose Dulbecco's modified Eagle's medium (Thermo Fisher Scientific, Waltham, MA, USA) supplemented with 10% (v/v) fetal bovine serum (Thermo Fisher Scientific, Waltham, MA, USA) and 1% (v/v) penicillin–streptomycin. The cells were kept at 37°C in a humidified 5% CO_2 incubator and cultures beyond passage 25 were discarded. The human embryonic stem cell (hESC) lines H1 (WA01, WiCell; RRID: CVCL_9771) and PDX1EGFP/+ HUES4, acquired from our facility (Ameri *et al.*, 2017), were cultured in DEF-CS culture media (Takara Biosciences, San Jose, CA, USA) according to the manufacturer's guidelines. The culture medium was changed daily, and cells were passaged every 2–3 days using TrypLE Express Enzyme (Thermo Fisher, Waltham, MA, USA). All cell cultures were maintained in a humidified incubator at 37°C with 5% CO_2. Culturing the hESC lines H1 and HUES4 was done in accordance with relevant guidelines and regulations and after consent from the regional scientific ethical committee of the Capital Region of Denmark (protocol nr.: H-21043866; appendix 94634).

Cell- and viability count

HEK293 cells were plated in 60 mm petri dishes (≈20% confluency) and HuES4 and H1 cells were seeded in 12-well cell culture dishes with a density of 15 000 cells per well. After 24 h of settling, cells were treated with either DMSO (control) (Sigma/Merck, Darmstadt, Germany) or APAP (HEK293: 500 µM, HuES4 and H1: 200 µM), for 24, 48, or 72 h. To detach the cells, Trypsin or TrypLE Express Enzyme (Thermo Fisher, Waltham, MA, USA) was used. The cells were then centrifuged at 250*g* for 5 min, resuspended in 1 ml of culture medium, and counted. HuES4 and H1 cell counting was performed on quadruplicate technical replicate wells. The counting process was performed with Via1-Cassettes™ (ChemoMetec, Lillerød, Denmark) and a NucleoCounter® NC-200™ (ChemoMetec, Lillerød, Denmark) automated cell counter following the manufacturer's protocol and resulted in measurement of total number of cells and the percentage of viable cells. All three cell lines were analyzed at a ≈80% confluency to avoid restricted growth and to ensure that the analyses were performed on cells within their exponential growth phase.

Flow cytometric analysis of HEK293, HuES4, and H1 cell lines

HEK293, HuES4, and H1 cell lines were plated and left to settle for 24 h prior to treatment with control (DMSO) or APAP (HEK293: 500 µM; HuES4 and H1: 200 µM) for 48 h. The cells were detached, fixed by slowly adding ice-cold 70% (v/v) ethanol while gently vortexing the tube, and left overnight in the fridge at 4°C. After centrifugation and removal of the supernatant, the pellet was resuspended in PBS containing 0.25% (v/v) Triton X-100 and incubated on ice for 15 min to permeabilize the cells. The cell pellet was then incubated for 30 min in the dark at room temperature (RT) with PBS containing 10 µg/ml RNase A (diluted from a stock 10 mg/ml RNase A (Sigma/Merck (R-5000), Darmstadt, Germany) in 10 mM Tris pH 7.5, 10 mM $MgCl_2$) and 20 µg/ml propidium iodide (diluted from a stock 3.6 mg/ml propidium iodide (Sigma/Merck, Darmstadt, Germany) in DMSO). After DNA staining, the cells were loaded and analyzed on a FACSverse multicolor flow cytometer using the FACSuite software (BD Bioscience, San Jose, CA, USA). Cells were gated according to forward-scatter/side-scatter (FSC/SSC) principles, followed by an FSC-A/FSC-H to ensure the analysis of single cells. Approximately 6000–10 000 cells were analyzed per condition. For an unbiased analysis of the cell cycle profile the Flowing Software 2.5 (Turku Bioscience Centre, Turku, Finland), automated cell cycle tool was used to define the distribution of cells within the different cell cycle stages, G1/G0, S, and G2/M. All three cell lines were harvested at a 70–80% confluency to avoid restricted growth and to ensure that the analyses were performed on cells within their exponential growth phase.

DNA replication analysis

Click-iT® Plus 5-ethynyl-2′-deoxyuridine (EdU) Pacific Blue® Flow Cytometry Assay Kits (Thermo Fisher Scientific, Waltham, MA, USA) were used to measure *de novo* DNA synthesis according to the manufacturer's protocol. Briefly, HEK293, HuES4, and H1 cell lines were plated and left to settle for 24 h prior to treatment with control (DMSO) or APAP (HEK293: 500 µM; HuES4 and H1: 200 µM) for 3 h with the addition of 10 µM EdU for the final 2 h. Cells were loaded and analyzed on a FACSverse multicolor flow cytometer using the FACSuite software (BD Bioscience, San Jose, CA, USA). Cells were gated according to FSC/SSC principles, followed by an FSC-W/FSC-H to ensure the analysis of single cells. The cell cycle profiling setup was initially validated using HEK293 cells exposed to L-Mimosine (Sigma/Merck, Darmstadt, Germany), an effective inhibitor of S-phase entry (see Supplementary Fig. S1). Approximately 6000–10 000 cells were analyzed per condition. For the detection of EdU Pacific Blue®, a 405-nm excitation filter with a violet emission filter (448/45) was used.

High-resolution mass spectrometry of APAP metabolites

Media samples from HEK293 cells cultured for 72 h with 500 µM APAP or control (DMSO) were prepared as described previously (David *et al.*, 2021). Briefly, media samples (100 µl) were diluted to 1 ml of HPLC grade water, acidified with 1% (v/v) formic acid, and extracted using Strata-X SPE (Phenomenex, Le Pecq, France). Extracts were analyzed on a Bruker timsTOF Pro2 with the VIP-HESI source, interfaced with a Bruker Elute2 chromatographic system (Bruker Daltonik, Bremen, Germany). Compound chromatographic separation was achieved using an ACQUITY UPLC HSS T3 (Waters Technologies, Saint Quentin, France) (1.8 µm 2.1 × 150 mm) maintained at 40°C. Injection volume was set at 2 µl. Flow rate was set at 300 µl/min with mobile phases of ultrapure water/0.1% (v/v) formic acid (A) and acetonitrile/0.1% (v/v) formic acid (B). The gradient was as follows: 0 min, 99% A (0.3 ml/min); 0–10 min, linear from 99% to 45% A (0.3 ml/min); 10–15 min, linear from 45% to 0% A (0.3 ml/min); 15–20 min, 0% A (0.6 ml/min); 20–20.5 min, linear from 0% to 99% A (0.6–0.3 ml/min); 20.5–23.5 min, 99%A (0.3 ml/min). Source parameters were as follows: end plate offset 500 V, capillary tension 3600 V, nebulizer pressure 2.2 bars, dry gas 10.0 l/min, dry temperature 220°C. Data were acquired using a data-dependent acquisition (DDA) Parallel Accumulation Serial Fragmentation (PASEF) method, in—and +ESI modes, with the following parameters: m/z range 20–1300, two PASEF scans at 20 and 50 eV, target intensity 4000, intensity threshold 100, active exclusion enabled for 0.1 min and released after intensity has doubled, calibration with sodium formate clusters. To evaluate and control for potential background contaminants, one workup sample (i.e. extraction with HPLC grade water instead of sample) per analytical batch

was prepared and injected. To ensure there was no presence of remaining traces in the chromatographic system from previous batches, solvent blank samples (acetonitrile/H2O (20:80)) were also injected within the analytical batch. A suspect list including APAP parent compound and its metabolites (13 in total) found in our previous study was screened in all samples (exposed to APAP and DMSO controls) (David *et al.*, 2021). The identities of the expected APAP metabolites were determined from accurate mass, isotopic fit, and fragmentation data obtained from DDA-PASEF acquisition and from comparison with standard compounds (David *et al.*, 2021). Metabolite annotation was based on recommendations by (Schymanski *et al.*, 2014) (Supplementary Table S1). Peak integration of all detected compounds was performed manually using the vendor Bruker-supplied DataAnalysis tool to ensure accuracy.

Mouse models

Mouse embryo culture and transfer model

Experiments were performed under license number 2021-15-0201-00851 from the Danish Animal Experiments Inspectorate and under EU directive 2010/63/EU on the protection of animals used for scientific purposes. For the mouse embryo collection and *ex vivo* culture, experiments were performed with inbred C57BL/6JRj and outbred CD1 (RjOrl: SWISS) dams as embryo donors. For experiments with *ex vivo* culture and subsequent embryo transfer, inbred C57BL/6JRj females were used as embryo donors and outbred CD1 (RjOrl: SWISS) were used as embryo recipients. Mice were kept in individually ventilated cages at a temperature of 22°C (±2°C), with a humidity of 55% (±10%), under 12/12-h light/dark cycles. Embryos were harvested from prepubescent (4- to 5-week-old) C57BL/6JRj females. The donor females were subjected to a hormone treatment before mating that consisted of an intraperitoneal injection of 5 IU/female of Pregnant Mare Serum Gonadotropin (Prospec, Rehovot, Israel,), followed 47 h later by a second intraperitoneal injection of 5 IU/female of hCG (Chorulon Vet, ref. 422741). After the second injection, each female was set in cross with a C57BL/6JRj stud male. The following morning, mating was monitored by the observation of copulation plugs in the vagina of the females. The day of plug detection was considered embryonic day 0.5 (E0.5). Two-cell-stage embryos (E1.5) were harvested 1.5 and morulae 2.5 days post-coitum (dpc). On the day of dissection, pregnant females were sacrificed by cervical dislocation and immediately after the oviducts were dissected and placed on a petri dish containing M2 medium (Sigma/Merck, Darmstadt, Germany, ref. M7167). Embryos were flushed out of the oviduct using a blunt 30G needle attached to a 1 ml syringe filled with M2 medium. Embryos were collected from the eluted medium using a 115 μm diameter glass capillary (Retransferpipette, Biomedical Instruments, Zöllnitz, Germany) attached to a mouth-pipetting system (Mouthpipette, Biomedical Instruments, Zöllnitz, Germany) and washed through three 50 μl drops of M2 medium. Finally, embryos were moved to a fresh petri dish and placed in a 50 μl drop of KSOM medium (Embyomax KSOM + AA, Merck Millipore, Burlington, MA, USA, ref. MR-106-D) without antibiotics covered by sterile mineral oil (NidOil, NordicCell, Copenhagen, Denmark, ref. 90142). Embryos were cultured for either 24 or 48 h at 37°C, 5% $C0_2$, in KSOM only (control groups) or in different concentrations of APAP diluted in KSOM. All experiments were performed with APAP dissolved directly in culture media without any changes in osmolarity (data not shown). Light microscopy (LM) images of embryos were taken immediately after exposure and before the embryos were fixed in 4% (w/v) paraformaldehyde (PFA). Experiments involving cleavage-stage embryos were conducted separately for 10 and 25 μM APAP, each with respective controls, in one independent experiment. Exposure groups ranging from 50 to 200 μM APAP, again with respective controls, were included in a second independent experiment. Mouse blastocyst-stage embryo experiments were conducted as two independent experiments with appropriate controls.

For embryo transfer to pseudo-pregnant recipient dams, 10- to 12-week-old CD1 females in anestrus were stimulated to enter the cycle by setting them in cross with vasectomized CD1 males. Formation of vaginal plug was monitored every morning for 3 days. Dams that showed a plug on the third day of breeding were selected as pseudo-pregnant females and used to perform the embryo transfer of the cultured embryos. The dam was anesthetized by an intraperitoneal injection of 20 mg/ml Avertin from a stock solution of 1 g Tribromoethanol (VWR chemicals, Radnor, PA, USA, ref. ACRO421430500) diluted in 630 μl 2-methyl-2-butanol (Sigma/Merck, Darmstadt, Germany, ref. 240486). One hundred and twenty microliters of this stock were diluted up to 10 ml in isotonic saline to obtain the ready-to-use solution at a dose of 25 μl/g. Depending on the embryonic stage, 10–12 embryos were transferred to each oviduct (morula stage embryos) or uterine horn (blastocyst-stage embryos) of the pseudo-pregnant dam. The embryo transfer was performed according to the standard procedure described in (Johnson, 1986). Control embryos were always transferred to the right oviduct/uterine horn, and APAP-exposed embryos to the left oviduct/uterine horn. Eighteen days after the transfer (embryonic day E18.5), the pregnant dams were euthanized and dissected to count the number of fetuses developed in each uterine horn.

Mouse pregnancy model

Experiments were performed under license number 2023-15-0201-01548 from the Danish Animal Inspectorate and under EU directive 2010/63/EU on the protection of animals used for scientific purposes. C57Bl/6JBomTac mice (Taconic, Lille Skensved, Denmark) arrived at the animal facility at 7–8 weeks of age. Experiments were run in two independent cohorts of 24 females and 12 males. Upon arrival, females were housed in 12 boxes of two and males six-by-six. Otherwise, housing and environment were as described previously (Ernstsen *et al.*, 2021). Mice were acclimatized 2 weeks prior to starting the experiments. On the day of experiment initiation, one male was introduced to two dams in one home cage and the following day (Day 1) APAP administration was initiated. Female cages were allocated by draw to either 200 mg/kg/day APAP administrated as a single daily oral gavage in tap water or tap water (vehicle control) for a total of 10 days (Days 1–10). Females sharing cages received the same treatment and dosing based on body weight on Day 0. Males were separated from females on Day 5 to avoid further breeding. After end administration at Day 10, dams were transferred to clean cages. Dams were euthanized on Day 18 and number of fetuses and placental resorptions counted blindly by two experienced veterinarians. Three controls and two APAP dams were excluded due to lack of pregnancy (ctrl 3, APAP 2).

APAP concentrations in female reproductive tract

All materials were sampled at the Copenhagen University Hospital, Denmark, Copenhagen Fertility Clinic and TFP Stork Fertility Clinic, Denmark, in accordance with relevant guidelines and regulations and after consent from the regional scientific ethical committee of the Capital Region of Denmark (protocol nr.: 17003845). All material was anonymized and collected as part of standard clinical procedures.

Follicular fluid

Follicular fluid was collected from a total of 26 women during transvaginal ultrasound-guided aspiration of the pre-ovulatory follicles. The procedure is part of standard fertility treatment with the aim of collecting oocytes, termed oocyte pickup (OPU). As a by-product of OPU, follicular fluid is recovered but is routinely discarded. Each patient scheduled for OPU receive, as part of pain-management 1 g of APAP 1 h before OPU. Collected follicular fluids were centrifuged and stored at −20°C until analysis. For measurements of APAP concentration in follicular fluid, we only evaluated samples without blood contamination collected from the first follicle aspirated that was greater than 20 mm in diameter (pre-ovulatory).

Endometrial tissue and uterine fluid

Endometrial tissue and uterine fluid were collected from seven women as part of an endometrial scratching (ES) procedure. ES can be performed as part of fertility treatment to patients with recurrent implantation failure and has been suggested to improve chances of implantation (Van Hoogenhuijze *et al.*, 2019; Iakovidou *et al.*, 2023). Endometrial tissue and uterine fluid were recovered during ES but are routinely discarded. Each patient scheduled for ES received as part of pain management 1 g of APAP 1 h before the procedure. Following intrauterine placement of an inner and outer biopsy catheter, a small amount of suction was applied. The inner catheter was removed and brought to the laboratory for collection of uterine fluid. A new inner catheter was then positioned, and endometrial biopsy/scratching was performed by moving the catheter while applying strong suction with a syringe. In the laboratory, the initial inner catheter was rinsed with 0.4 ml of sterile saline to recover the approximately 5–10 µl of uterine fluid collected. Fluid from the first inner catheter and endometrial tissue from the second catheter were stored at −20°C until analysis.

Liquid chromatography–mass spectrometry measurements for APAP

For measurements of APAP in follicular fluid, 200 µl aliquots of follicular fluid, calibration standards (10 solutions of native APAP standard diluted in water in the concentration range from 0.5 to 2000 ng/ml), and control materials (native APAP spiked in urine pool in three different concentrations) were added to 20 µl of internal standard solution followed by 276 µl NH_4Ac-buffer. Immediately before enzymatic de-conjugation, all sample extracts, calibration, and control materials were combined with 10 µl of freshly prepared enzyme mixture (ß-glucuronidase from *Escherichia coli* K12, sulfatase from *Aerobacter aerogenes*, and NH_4Ac-buffer; 1:1:3), mixed, and incubated at 37°C for 3 h, stored overnight at −20°C and then centrifuged (18 213*g*) at 4°C for 10 min. Supernatants were transferred to HPLC vials and were then ready for analysis.

For uterine fluid and endometrial tissues, APAP was extracted from approximately 100 mg of diluted uterine fluid (98.9–120 mg) and endometrial tissue (35.2–141 mg) samples following a validated method for extraction of chemicals (Artacho-Cordón *et al.*, 2017). Briefly, samples were mixed with 20 µl of internal standard solution (containing 200 ng/ml of APAP-d4 and 100 ng/ml $^{13}C_4$-methylumbelliferone including 4-methylumbelliferyl b-D-glucuronide and 4-methylumbelliferyl-b-D-sulfate dissolved in 50% (v/v) methanol), then centrifuged and stored at RT for 30 min. Samples were submerged by addition of 1 ml acetone and mechanically homogenized with a mixer. The mixer was then washed with 2 ml methanol per extract, which was collected and added to the homogenized extract. Then the extracts were sonicated in an ultrasound bath for 10 min. Subsequently, total extract volumes were reduced to <2 ml each by evaporation under a gentle nitrogen stream at RT. Thereafter, tissue residuals were removed by transferring the remaining extracts to a 2 ml Eppendorf tube followed by storing at −20°C for 15 min and then centrifugation (18 213*g*) at 4°C for 10 min. Supernatants were then transferred to new glass tubes, evaporated to dryness under a stream of nitrogen, and re-suspended in 496 µl 0.5 M ammonium acetate (NH_4Ac) buffer (pH5.5).

The total (free and conjugated) content of APAP in the sample extracts was measured by isotope diluted online-TurboFlow-liquid chromatography-mass spectrometry (LC-MS/MS) using a Thermo Scientific Aria TLX-1 LC system coupled to a TSQ Ultra triple quadrupole mass spectrometer equipped with a heated electrospray ionization source running in positive mode. The instrument was used in combination with Aria operating software 1.6.3 and Xcalibur 2.1.0.1139 system software (ThermoFinnigan, Bellefonte, PA, USA). The TurboFlow-LC systems were equipped with a loading column; TurboFlow Cyclone P column, 0.5×50 mm (Thermo Scientific) followed by an analytical Gemini-C18 column, 3 µm particle size, 3×50 mm (Phenomenex). Prepared batches were kept on the auto-samplers at 10°C. The injection volume was 100 µl. Flow rate and loading and eluting gradients were specified for this specific method and the mobile phases used were loading solvents; A: 10 nM NH_4Ac, B: 0.1% (v/v) formic acid in methanol, C: acetone/isopropanol/acetonitrile 10:45:45 and eluting solvents; A: 3 nM ammonium hydrogen carbonate, B: acetonitrile. The method was validated, and limit of detection was determined (LOD = 0.48 ng/ml) for urinary APAP as previously described (Rehfeld *et al.*, 2022) according to the ICH guidelines (ICH, 2005). The sample extracts were analyzed in one batch, also including standards for calibration curves, three blanks, and three times three-spiked urine pool controls followed by one batch more with samples diluted to fit the method calibration range. The relative standard deviation in the three control levels ranged from 2.7% to 7.6%. For the LC-MS/MS analyses, native APAP (N-acetyl-4-aminophenol, CAS No. 103-90-2 procured from Sigma-Aldrich), labeled APAP-d4 (Paracetamol-D_4, CAS No. 64315-36-2 procured from LoGiCal®) and all other reagents and solvents were of analytical, HPLC or MS grade, and all chemicals and laboratory equipment were tested for contamination before utilization.

Human embryogenesis experiments

All experiments were performed in accordance with relevant guidelines and regulations and conducted at the Copenhagen University Hospital—Hvidovre and Copenhagen University Hospital—Rigshospitalet, Denmark. Surplus human embryos from fertility treatment were donated at Copenhagen University Hospital—Rigshospitalet, Copenhagen University Hospital—Hvidovre, TFP Stork Fertility Clinic, and Copenhagen Fertility Center between the years 2020 and 2023. The study protocol was approved by the Research Ethics Committee of the Capital Region of Denmark (H-19050437) with signed informed patient consent given prior to donation. A total of 22 cleavage-stage embryos and 68 blastocyst-stage embryos were used. All experiments were performed with APAP dissolved directly in SAGE-1-Step culture media without any changes in osmolarity (data not shown) with gentamicin as an antibiotic. APAP was purchased from Sigma Cat. No. A5000 (Sigma/Merck, Darmstadt, Germany) for these experiments and all subsequent experiments in the study.

Cleavage-stage embryos

Cleavage-stage embryos were frozen at D2 or D3 after fertilization and thawed using a slow freeze protocol (Freezekit and ThawKit Cleave Vitrolife, Göteborg, Sweden) as described by the manufacturer (https://www.vitrolife.com/globalassets/support-documents/short-protocols/sp_slow_freeze_cryopreservation_Cleavage.pdf). Following thawing, embryos were placed in equilibrated SAGE 1-Step media (CooperSurgical Fertility Solutions, Ballerup, Denmark) drops covered with mineral oil (Origio, CooperSurgical Fertility Solutions, Ballerup, Denmark) at 37°C under 6% CO_2 and 5% O_2. Within 2 h after thawing, embryos were matched in pairs and allocated to exposure groups (100 or 200 µM APAP) or control group according to a prioritized order of the following parameters: (i) female origin (sibling embryos), (ii) female age at time of embryo cryopreservation, (iii) time of cryopreservation (D2 or D3), (iv) and number of blastomeres and morphology after thawing. This was done to minimize differences between control and APAP-exposed embryos. Experiments were performed using a timelapse incubator (EmbryoScope ESD Vitrolife, Göteborg, Sweden). As the specific cryopreservation time of the individual D2 embryos was unknown, the start point depicted in time-lapse videos (Videos 1 and 2) were estimates of embryo age after fertilization. Cleavage-stage embryo experiments were performed in two independent experiments with 100 and 200 µM APAP, along with respective controls.

Blastocyst-stage embryos

Embryos were vitrified at D5 or D6 and subsequently thawed (Vit Kit Freeze NX and Vit Kit®-Warm, Irvine Scientific, Santa Ana, CA, USA) as described by the manufacturer (https://www.irvinesci.com/media/IrvineScientific/Resources/0/0/002773_warming_ooctyes_protocol.pdf). One embryo did not survive the vitrification and warming process and was therefore excluded from the experiments. Embryos were subsequently transferred to a pre-equilibrated dish with 25 µl drops of SAGE 1-Step culture media (CooperSurgical Fertility Solutions, Ballerup, Denmark) and cultured at 37°C under 6% CO_2 and 5% O_2. Within 3 h after warming, embryos were matched in pairs and allocated to exposure groups (100 or 200 µM APAP) or control group according to a prioritized order of the following parameters: female origin (sibling blastocysts), female age at the time of vitrification, day of vitrification (D5 or D6), and morphology post-warming. A maximum of 12 embryos were warmed per experiment by two experienced embryologists to reduce difference in culture time between warming and experiment initiation. Morphology was evaluated by LM following warming, at start of the experiment, following 3 h of APAP exposure, and at the end of the 6 h culture period using the Gardner grading system (Gardner et al., 2000) (Supplementary Tables S2 and S3). Blastocyst-stage embryo experiments were performed in three independent experiments with 100 or 200 µM APAP, along with respective controls.

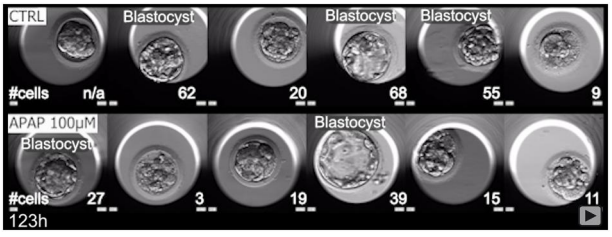

Video 1. Paracetamol (N-acetyl-para-aminophenol, APAP) affects cell number and blastocyst rate in human embryos. Time-lapse video of human cleavage-stage embryos cultured with either control media (CTRL) or 100 µM APAP. Embryos were thawed at 48 or 72 h of development and subsequently cultured for an additional 75 or 51 h, respectively, until reaching 123 h of development. The cell number in each embryo after 123 h of development is indicated in the lower right corner of each video frame.

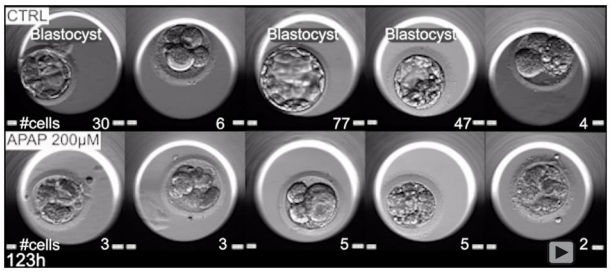

Video 2. Paracetamol (N-acetyl-para-aminophenol (APAP)) affects the cell number and blastocyst rate of human embryos. Time-lapse video of human cleavage-stage embryos cultured with either control media (CTRL) or 200 µM APAP. Embryos were thawed at 48 h of development and subsequently cultured for an additional 75 h until reaching 123 h of development. The cell number in each embryo after 123 h of development is indicated in the lower right corner of each video frame.

Whole-mount immunofluorescence staining of human blastocyst-stage embryos

Click-iT® Plus EdU Alexa Fluor® 555 Cell Proliferation imaging kit (Thermo Fisher Scientific, Waltham, MA, USA) was used to visualize and quantify newly synthesized DNA. APAP was diluted in equilibrated SAGE 1-Step media and dishes made with 25 µl culture media drops with or without APAP (100 or 200 µM) covered in mineral oil (Origio, CooperSurgical Fertility Solutions, Ballerup, Denmark) and maintained in the incubator for minimum 2 h to equilibrate before experiment start. Embryos were exposed to 100 or 200 µM APAP and control in SAGE 1-Step media for 6 h with the addition of 10 µM EdU for the final 3 h. After treatment, the embryos were subjected to a modified procedure of the protocol from (Wong, 2021) combined with the manufacture protocol of the Click-iT® Plus EdU Alexa Fluor® 555 Cell Proliferation imaging kit. In brief, embryos were fixed individually in Millicell® (Sigma/Merck, Darmstadt, Germany) cell culture inserts in 4% (w/v) PFA (VWR chemicals, Radnor, PA, USA) for 15 min at RT. Next, the embryos were washed twice in 3% (w/v) BSA in PBS before placed in 0.5% (v/v) PBSTr for 20 min at RT. Again, the embryos were washed twice in 3% (w/v) BSA in PBS and placed in Click-iT® Plus reaction cocktail for 30 min. The embryos were protected from light for the remainder of the protocol and were washed once in 3% (w/v) BSA in PBS before being transferred to neutralization buffer and incubated for 15 min at RT. Embryos were then subjected to washes, primary- and secondary antibodies, and mounted as described under 'Whole-mount immunofluorescence staining of human and mouse embryos'. Segregation between the inner cell mass (ICM) and TE fates was determined by the expression of OCT3/4 and CDX2 (Niwa et al., 2005; Niakan and Eggan, 2013). A definable ICM was identified by a clear cluster of cells exclusively expressing OCT3/4. An indefinable ICM was defined by either no OCT3/4 positive cells, OCT3/4 positive cells dispersed throughout the blastocyst-stage embryos with no cluster or a cluster of cells expressing both CDX2 and OCT3/4.

Whole-mount immunofluorescence staining of human and mouse embryos

The whole-mount immunofluorescence staining of embryos was performed following a procedure modified from (Wong, 2021). In brief, pre-implantation embryos were fixed in 4% (w/v) PFA (VWR

chemicals, Radnor, PA, USA) for 15 min at RT with human embryos fixed individually using Millicell® (Sigma/Merck, Darmstadt, Germany) cell culture inserts. Next, the embryos were placed in 0.5% (v/v) PBSTr (0.5% Triton X-100 (Sigma/Merck, Darmstadt, Germany) in PBS) for 20 min at RT and then transferred to neutralization buffer (1M Glycine in 0.1% (v/v) PBSTr) and incubated for 15 min at RT. The embryos were then washed three times in 0.01% (v/v) PBSTw (0.01% Tween-20 (Sigma/Merck, Darmstadt, Germany) in PBS) for 10 min at RT. After the last wash, the embryos were transferred to a well containing blocking buffer (3% (v/v) donkey serum and 1% (w/v) BSA (Sigma/Merck, Darmstadt, Germany) in PBSTw) and incubated in a humidified box containing wet tissue paper at 4°C overnight. The embryos were then transferred to primary antibodies diluted 1:200 in blocking buffer and incubated for 2–3 days at 4°C. The embryos were then washed 3 times in 0.01% (v/v) PBSTw for 10 min at RT. The embryos were then transferred to a well with secondary antibodies diluted 1:500 in blocking buffer (DAPI diluted 1:5000 or phalloidin diluted 1:100) and incubated, in the dark, at RT for 3–4 h. Afterward, the embryos were washed 3 times in 0.01% (v/v) PBSTw for 10 min at RT before being transferred to a coated microscope slide (Dako Agilent, Glostrup, Denmark). The slides were left to dry for a few minutes at RT, in the dark, before addition of 10 µl of mounting medium (90% (v/v) glycerol and 2% (w/v) n-propyl gallate in PBS) and mounting with cover glasses (VWR, Radnor, PA, USA) (Kiprilov *et al.*, 2008). The cover glass edges were sealed with transparent nail polish. Due to the size of the material, unfortunately, some embryos were lost during the multiple steps in the whole-mount immunofluorescence staining protocol.

Immunofluorescence microscopy and imaging

The immunofluorescence and differential interference contrast images were obtained using an Olympus BX63 upright microscope with an Olympus DP72 color, 12.8-megapixel, 4140 Å∼3096 resolution camera (Olympus, Tokyo, Japan). Olympus CellSense Dimension software version 1.7 (Olympus, Tokyo, Japan) was used for deconvolution and 3D reconstruction of Z-stacks as previously described (Schmid *et al.*, 2018). Images were later processed in ImageJ (Bethesda, MD, USA) and Adobe Photoshop CS6 (Adobe, San Jose, CA, USA). Quantification of the EdU intensity was performed blinded with an outline drawn around each cell double positive for OCT3/4 and EdU. Only cells or parts of cells that did not overlap with other cells were included. Using the measurement and region of interest function in the CellSens dimension software (Olympus, Tokyo, Japan), the mean red fluorescence intensity was measured along with a background reading. The corrected mean fluorescence for the individual cells was subsequently calculated by subtracting the corresponding background value. The following primary antibodies were used at a 1:200 dilution: rabbit anti-CDX2, No. D11D10 (Cell Signaling Technology, Danvers, MA, USA), goat anti-OCT3/4, No. sc-8629 (Santa Cruz Biotechnology, Dallas, TX, USA), mouse-GATA4, No. sc-25310 (Santa Cruz Biotechnology, Dallas, TX, USA), and mouse anti-α-Tubulin, No. T5168 (Merck/Sigma-Aldrich, Darmstadt, Germany). Secondary antibodies (all from Thermo Fisher Scientific, Waltham, MA, USA) were used at a 1:500 dilution: Donkey-anti-mouse IgG Alexa Fluor® 568, Donkey-anti-rabbit IgG Alexa Fluor® 568, Donkey-anti-goat IgG Alexa Fluor® 488, and Donkey-anti-rabbit IgG Alexa Fluor® 647. F-actin and nuclei were stained with Phalloidin (Alexa Fluor® 488 or 568, Thermo Fisher Scientific, Waltham, MA, USA) and DAPI (Thermo Fisher Scientific, Waltham, MA, USA), respectively.

Data analysis and statistics

Data analyses were performed with GraphPad Prism 9 (San Diego, CA, USA), except for the Fisher–Freeman–Halton and Phi and Cramer's tests that were performed in SPSS 29.0.1.0 (Chicago, IL, USA). For the cell cultures, the 'n' signifies biological replicate experiments obtained from different passages. For mouse and human embryo culture experiments, individual embryo was considered as one n. For animal studies, each animal was considered as one n. For the measurement of APAP concentrations in the female reproductive tract, the 'n' signifies the number of donors. The specific statistical test used to analyze the given data is stated in the figure legends. Data are represented as the mean ± SD or SEM and $P < 0.05$ was considered statistically significant. All data supporting the findings of this study are available within the paper and its Supplementary Data.

Results

APAP inhibits ribonucleotide reductase and proliferation in yeast

APAP has been reported to cause DNA replication stress presumably through inhibition of ribonucleotide reductase (RNR) (Hongslo *et al.*, 1990), an essential enzyme for DNA synthesis that reduces ribonucleotides to 2′-deoxyribonucleotides, the building blocks of DNA. As RNR is highly conserved across the eukaryotic kingdom (Zhao *et al.*, 2000), we tested the effect of APAP on RNR in three strains of fission yeast *S. pombe*, a model organism that does not express pharmaceutical APAP targets such as prostaglandin-endoperoxide synthases (PTGS1 and PTGS2) and cannabinoid receptor 1 (CB1) (Wood *et al.*, 2012). The first strain was deleted for the *ddb1*-gene (*ddb1*Δ), which results in reduced 2′-deoxyribonucleotide pool and increased sensitivity to chemical RNR inhibition as compared to wild-type (WT) cells. The second strain was deleted for both the *ddb1*-gene and the RNR inhibitory gene *spd1* (*ddb1*Δ *spd1*Δ), which results in increased RNR activity and thus a ≈2-fold increased 2′-deoxyribonucleotide pool as compared to WT cells. The third strain was deleted for the *ddb1*-gene together with an activating point mutation in the large RNR subunit encoding gene *cdc22* (*ddb1*Δ *cdc22-D57N*), resulting in a ≈5-fold increased 2′-deoxyribonucleotide pool as compared to WT cells (Fleck *et al.*, 2013). The RNR-restricted *ddb1*Δ strain had decreased proliferation at 40- and 60 mM APAP as compared to WT. In contrast, this effect on cell division was suppressed in both the *ddb1*Δ *spd1*Δ and *ddb1*Δ *cdc22-D57N* strains with increased RNR activity (Supplementary Fig. S2a).

It has been proposed that APAP might interfere with RNR function through two possible mechanisms: (i) by quenching the tyrosyl free radical (Y122) in the cofactor site of the β subunit (β-RNR) or (ii) by forming an adduct between RNR and APAP's electrophilic metabolite, N-acetyl-p-benzoquinone imine (NAPQI) (Hongslo *et al.*, 1990) (Supplementary Fig. S2b). Since it is believed that yeast cells do not produce NAPQI (Srikanth *et al.*, 2005), we performed *in silico* modeling using a 3D model of β-RNA from *S. pombe*. These analyses showed that APAP likely binds to the *S. pombe* β-RNR cofactor site in proximity of the tyrosyl free radical and is stabilized through π–π stacking interactions, hydrophobic interactions, and hydrogen bonds (Supplementary Fig. S2c–e). The binding of APAP in β-RNR might facilitate the disruption of the tyrosyl free radical by inhibiting the formation of the tyrosyl radical through competition, resulting in a phenoxyl radical (Supplementary Fig. S2c, inset), or by interfering with the redox potential of the di-nuclear iron center in the cofactor site.

To understand the effect of APAP on human RNR, we used a recombinant *S. pombe* strain with the native RNR coding regions *cdc22* and *suc22* replaced with cDNA encoding the human orthologous *RRM1* and *RRM2* subunits (*hR1/R2*). Compared to the WT strain, this strain was more sensitive to APAP in terms of growth, both on solid agar and in liquid culture (Supplementary Fig. S2f and g; (g, n = 3)), correlating with accumulation of cells in G1- and S-phase (Supplementary Fig. S2h). Taken together, these data are consistent with an inhibitory action of APAP on RNR, resulting in disruption of cell cycle progression at the G1/S-border and through the S-phase.

APAP reduces DNA synthesis and proliferation in human somatic cells and embryonic stem cells

Next, we exposed human somatic embryonic kidney (HEK293) cells to 500 μM APAP. This exposure resulted in decreased total cell numbers in a time-dependent manner without effecting cell viability (Supplementary Fig. S3a and b, n = 6). The cells exposed to APAP displayed accumulation in the S phase of the cell cycle with a fold change of ≈1.5 as compared to the control (Supplementary Fig. S3c, n = 6, for raw data, see Supplementary Table S4), concomitantly with reduced *de novo* DNA synthesis (Supplementary Fig. S3d, ctrl: n = 5, APAP: n = 6).

hESCs are pluripotent cells derived from the ICM of a pre-implantation blastocyst-stage embryo and a validated model system of PID (Luz and Tokar, 2018). As we and others previously have found that standard exposure to APAP resulted in >100 μM concentrations in blood plasma (Langford *et al.*, 2016; Rehfeld *et al.*, 2022), we next exposed hESC lines H1 and HUES4 to 200 μM APAP. This resulted in similar effects in the two hESC lines as observed in the somatic HEK293 cells and yeast cells (Supplementary Fig. S3e, f, i, and j, n = 5), including a time-dependent reduction in the total cell number without affecting viability, S phase accumulation (Supplementary Fig. S3g and k, n = 5, for raw data, see Supplementary Table S4), and reduction of *de novo* DNA synthesis as compared to controls (Supplementary Fig. S3h and l, n = 4). In addition, we found a reduction of cells in the G2/M phase, reflecting accumulation in the S-phase. Taken together, these data suggest that APAP restricts cell proliferation via inhibition of DNA synthesis.

APAP and paracetamol sulfate were the predominate compounds after in vitro exposure

APAP is metabolized into multiple compounds through both oxidative and direct phase II conjugation pathways in the human body, incl. the cytotoxic compound NAPQI (David *et al.*, 2021; Gorrochategui *et al.*, 2023). To understand the metabolism of APAP *in vitro*, we exposed HEK293 cells to 500 μM APAP for 72 h. After screening for 13 known metabolites previously identified *in vivo* in the media from APAP-exposed cells (n = 3; Supplementary Fig. S4), only APAP and two metabolites, acetaminophen sulfate (APAP-S) and S-methyl-3-thioacetaminophen sulfate (S-CH_3-APAP-S), were identified. Importantly, APAP and APAP-S were the most abundant compounds, with APAP being approximately 60 times more prevalent than S-CH_3-APAP-S, derived from a NAPQI-glutathione conjugate (David *et al.*, 2021). Together with the data indicating no decrease in viability (Supplementary Fig. 3b), these results suggest that NAPQI is unlikely to be responsible for the accumulation of cells in the S-phase, again indicating a direct effect of APAP on RNR.

APAP disrupts early PID in mice

To determine the effect of APAP on PID, we investigated the effect of 24 or 48 h exposure (10–200 μM APAP) using C57BL/6 mouse 2-cell embryos (embryonic day (E)1.5). After 24 h of development, controls (n = 21) as well as embryos exposed to 10 μM (n = 12) consisted of the expected eight blastomeres, whereas embryos exposed to 25 μM (n = 11) had an equal distribution of four or eight blastomeres. All embryos exposed to 50–200 μM APAP (50 μM: n = 8, 100 μM: n = 6, 150 μM: n = 9, 200 μM: n = 6) consisted of two to four blastomeres, suggesting a delay in the second to third cleavage stages (Fig. 1a and d). After 48 h, most control embryos had developed into early or expanded blastocysts that were identified by a well-defined fluid-filled cavity (blastocoel). No embryos exposed to 50–200 μM (50 μM: n = 7, 100 μM: n = 10, 150 μM: n = 11, 200 μM: n = 8) developed beyond the early blastocyst stage and all had reduced cell number as compared to controls (n = 15) (Fig. 1a and e and Supplementary Fig. S5a). Blastomere morphology was not affected after 24 h of APAP exposure compared to control except for embryos exposed to 200 μM of APAP (n = 8); here a minority of embryos were amorphic with fragmented blastomeres (Fig. 1b).

Among embryos in the control group cultured for 48 h, we observed in general more OCT3/4-positive cells (marker for ICM) relative to CDX2-positive cells (marker for trophectoderm, TE) with some cells identified with both markers as expected for this developmental stage of lineage specification (Niakan and Eggan, 2013). Among the low APAP exposure groups (10–25 μM, 10 μM: n = 12, 25 μM: n = 11), we in general observed a similar differentiation of the ICM and TE with cells expressing both markers of ICM and TE. In contrast, APAP concentrations >25 μM displayed fewer blastomeres with exclusive TE (CDX2 positive) cells as compared to the control embryos (Fig. 1c). Moreover, APAP-exposed embryos displayed cell fragmentation and amorphic nuclei with increasing severity and frequency at the higher concentrations of 150 and 200 μM (Fig. 1c). Calculating a theoretical growth rate based on the 48 h experiments, we found that APAP delayed development, increasing cellular doubling time from ≈13 h for controls to ≈30 h for 200 μM APAP-exposed embryos (Fig. 1f). Moreover, delayed embryonic development was also reflected in a decreased blastocyst rate (Supplementary Fig. S5a).

To further substantiate the observations made in the inbred C57BL/6 mouse embryos, we next assessed the impact of a 48 h exposure to APAP at concentrations of 100 and 200 μM (n = 15) on PID using outbred CD1 mouse 2 cell embryos. Again, after 48 h, the control embryos initiated their development into early or expanded blastocysts, whereas none of the exposed embryos advanced beyond the early blastocyst stage (Supplementary Fig. S6a). Additionally, all exposed embryos exhibited a significantly reduced cell count compared to the controls (n = 15) (Supplementary Fig. S6b and c). These findings mirror the dose-dependent adverse effects of APAP exposure on PID observed in the inbred C57BL/6 mouse embryos. Together these experiments from both inbred and outbred mouse embryos demonstrate that APAP delays or disrupts embryonic development by reducing cell divisions in the mouse in a time- and concentration-dependent manner.

APAP reduces ICM in late PID in mice

To understand the effect of APAP during the later stages of PID, we exposed early C57BL/6 mouse blastocysts (E3.5) to 100 (n = 14), 150 (n = 21), and 200 μM (n = 26) APAP for 24 h. Most APAP-exposed embryos continued blastocyst development with a clearly defined expanded blastocoel, TE, and ICM (Fig. 2a) and with total cell numbers equivalent to those of controls (n = 26) (Fig. 2b and c). However, the number of cells in the ICM was decreased after 200 μM APAP (n = 19) as compared to controls (n = 15) (Fig. 2b and d); a phenotype that was recapitulated in

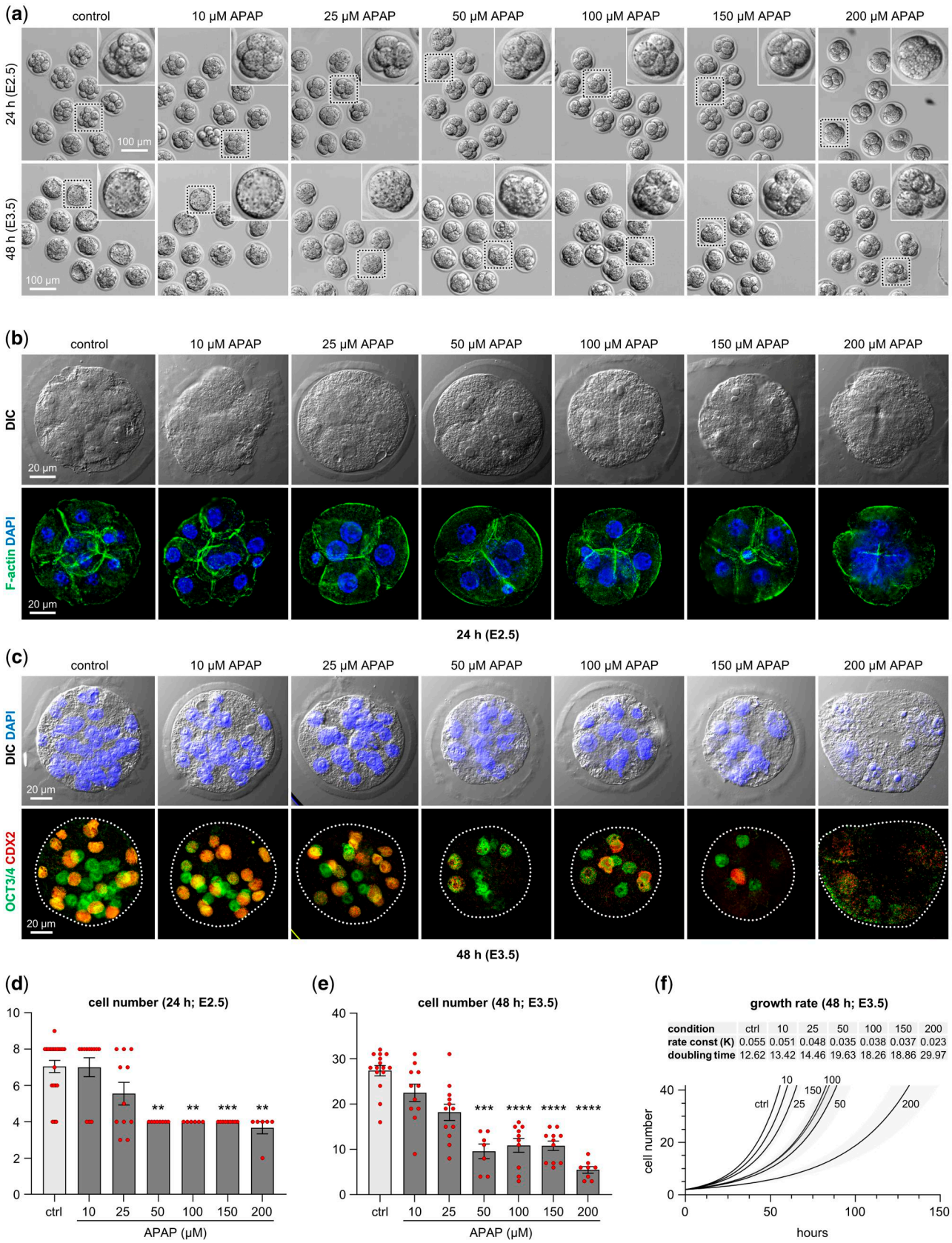

Figure 1. Mouse C57BL/6 early pre-implantation development is disrupted by paracetamol (N-acetyl-para-aminophenol (APAP)) exposure. (**a**) Representative light microscopy images of embryos cultured for 24 or 48 h in media (control) or media with APAP added at the stated concentrations. (**b**) Representative immunofluorescence microscopy (IFM) images of mouse embryos cultured for 24 h in media (control) or media with APAP at the stated concentrations. Upper panels: Differential interference contrast (DIC) analysis of the embryos. Lower panels: F-actin stained by Phalloidin (green) and the nuclei stained using DAPI (blue). (**c**) Representative IFM images of mouse embryos cultured for 48 h in control media or media with APAP at the stated concentrations. Upper panels: DIC analysis and DAPI nuclei staining (blue). Lower panels: trophectoderm cells (red) stained by anti-CDX2 antibody and inner cell mass cells stained by anti-OCT3/4 antibody (green). (**d**) Cell counts quantification based on IFM analysis of embryos

(Continued)

embryos stained for microtubules and F-actin, displaying reduced ICM size while the overall structural organization of cells was maintained (Fig. 2e). Taken together, these data suggest that APAP reduce the pool of pluripotent ICM cells during the final stage of PID (E3.5-E4-5).

APAP exposure during PID reduces pregnancy outcomes

As it is challenging to determine the exact concentration present within the reproductive tract of the mouse, translating doses from *in vitro/ex vivo* experiments (μM) to *in vivo* experiments (mg/kg/day) becomes complex. Therefore, we conducted C57BL/6 embryo transfers to pseudo-pregnant recipient dams after exposing 2-cell embryos (E1.5) *ex vivo* to understand whether human physiological relevant doses in plasma (100 and 200 μM) (Langford *et al.*, 2016; Rehfeld *et al.*, 2022) affected implantation and subsequent development. Exposed and control embryos were separately placed in each oviduct (morula stage embryos) or uterine horn (blastocyst-stage embryos) in equal numbers, depending on the duration of the exposure (24 or 48 h) (Fig. 3a). Exposure to APAP decreased implantation rates (significantly for all experiments except for 200 μM APAP for 24 h; $P = 0.1$) and the number of live fetuses (Fig. 3b–e). Prolonging the time *ex vivo* from 24 to 48 h increased the number of resorptions among the control dams. While exposure to APAP for 24 h decreased number of live fetuses and increased resorption points (Fig. 3b and c, 100 μM: n = 6, 200 μM: n = 7), suggesting that embryos implant but subsequently dies, the longer exposure of 48 h decreased both live fetuses and resorption points (Fig. 3d and e, 100 μM: n = 9, 200 μM: n = 11), indicating that the embryos had not implanted. These results suggest that disrupted PID after exposure to APAP impacts the ability of embryos to implant and/or survive after implantation.

To investigate the impact of *in vivo* exposure on PID and subsequent development, we gavaged C57/BL6 dams with APAP (200 mg/kg/day, single daily oral gavage) from 1 dpc and the subsequent 10 days. At cesarean section at 18 dpc, dams treated with APAP had reduced number of live fetuses. Moreover, post-implantation embryonic mortality increased following APAP exposure as determined by an increased number of resorption points as compared to the control group (Fig. 4a and b, ctrl: n = 21, APAP: n = 22). These *in vivo* results further underscore the impact of APAP exposure on the embryos, affecting both implantation and subsequent survival post-implantation.

APAP disrupts early human PID at therapeutic doses

To understand to what degree APAP enters the reproductive organs in women, follicular fluid (n = 26), endometrial tissue (n = 7), and uterine fluid (n = 7) were collected as part of routine procedures in the clinic from patients receiving a standard therapeutic dose of 1 g of APAP. One hour following administration, APAP had reached the follicular fluid at an average concentration of 38.1 μM, the endometrial tissue at an average of 80.3 μM, and the uterine fluid at an average of 124.5 μM. Notably, one woman had 291.3 μM in the uterine fluid (Fig. 5a).

To investigate the effect of APAP on human PID at concentrations present in the intrauterine environment after standard therapeutic doses, we exposed human cleavage-stage embryos to 100 and 200 μM APAP. For the exposure to 100 μM APAP, human development day 2 (D2) and D3 embryos (n = 6) were cultured for 48 or 72 h to reach D5 with corresponding controls (n = 6). For the exposure to 200 μM APAP, D2 embryos (n = 5) were cultured for 72 h to reach D5 with corresponding controls (n = 5). Results indicated that embryonic development in the APAP groups was compromised as compared to most of the controls (Videos 1 and 2; Fig. 5b and c—top panel; Supplementary Fig. S5b).

In embryos exposed to 100 μM APAP, the overall structural organization of the embryos appeared normal, but development was delayed as enumerated by reduced cell numbers as compared with controls (Fig. 5c—middle and lower panels). The concentration of 200 μM resulted in cells with fragmented nuclei indicating cell death (Fig. 4b—middle and lower panels). Quantifying the DAPI nucleus staining from each experiment, we observed a reduction in cell number of both 100 and 200 μM exposed embryos as compared to control (Fig. 5d and e). These data show that at concentrations present in the intrauterine environment after a standard therapeutic dose, APAP might disrupt early human PID either by delaying cell divisions or direct embryonic fatality.

APAP inhibits DNA synthesis and disrupts late human PID at therapeutic doses

To determine the effect of APAP on DNA synthesis *in situ* in late human PID, blastocyst-stage embryos D5–6 were exposed to APAP for 6 h (100 and 200 μM) with thymidine analog EdU added for the last 3 h to quantify DNA synthesis (Fig. 6a and e). The percentage of APAP-exposed embryos with a definable ICM was reduced as compared to controls (ctrl to 100 μM: n = 18, ctrl to 200 μM: n = 14) at a dose of 100 μM (n = 18) with a similar tendency observed with 200 μM (n = 15) (Fig. 6b and f).

Finally, we investigated DNA synthesis of OCT3/4 positive cells in the embryos with a definable ICM. We found no difference in number of OCT3/4 positive cells with incorporated EdU between embryos exposed to 100 μM APAP (n = 11) as compared with controls (n = 18) (Fig. 6c). However, we found that the level of EdU incorporation was reduced in the OCT3/4 positive ICM cells as compared with controls (Fig. 6d: control; n = 108 (108 cells from 18 blastocysts), APAP; n = 60 (60 cells from 11 blastocysts)). In the embryos subjected to 200 μM APAP (n = 9), the percentage of OCT3/4 positive cells with EdU incorporation was decreased (n = 12) (Fig. 6g). As with the 100 μM APAP exposure blastocyst, we found the level of EdU incorporation was reduced in the OCT3/4 positive ICM cells as compared to controls (Fig. 5h: control; n = 71 (71 cells from 11 blastocysts), APAP; n = 37 (37 cells from nine blastocysts)). Taken together, these results suggest that APAP exposure for 6 h negatively affected human PID at the blastocyst stage at physiological relevant concentrations through inhibition of DNA synthesis and proper expansion of ICM cells (for raw data, see Supplementary Tables S2 and S3).

Figure 1. Continued
cultured for 24 h in media (control; n = 21) or media with APAP at the stated concentrations (10 μM: n = 12, 25 μM: n = 11, 50 μM: n = 8, 100 μM: n = 6, 150 μM: n = 9, 200 μM: n = 6). (**e**) Quantification of cell numbers based on IFM analysis of embryos cultured for 48 h in media (control; n = 15) or media with APAP at the stated concentrations (10 μM: n = 11, 25 μM: n = 12, 50 μM: n = 7, 100 μM: n = 10, 150 μM: n = 11, 200 μM: n = 8). (**f**) The theoretical growth rate ($Y = Y0 \times \exp(k \times x)$) based on the 48 h cultivation experiment. The embryonic day in the parenthesis (e.g. E3.5) corresponds to their embryonic age at the end of the given exposure time. Statistical significance was tested with Kruskal–Wallis one-way analysis followed by Dunn's multiple comparison *post hoc* test (against control). Data points are represented as mean ± SEM. $^{**}P < 0.01$; $^{***}P < 0.001$; $^{****}P < 0.0001$.

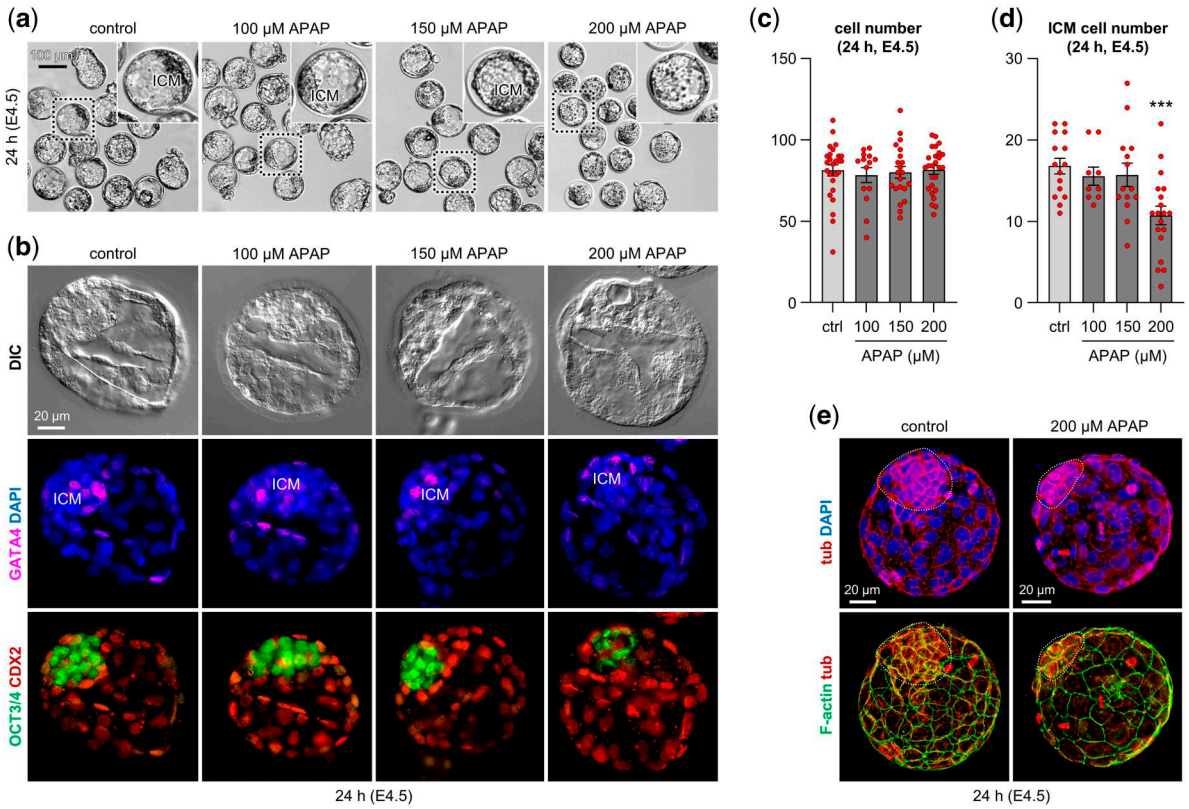

Figure 2. Mouse C57BL/6 blastocyst-stage development is disrupted by paracetamol (N-acetyl-para-aminophenol (APAP)) exposure. (**a**) Representative light microscopy images of late-stage blastocyst embryos cultured in media (control) or media with the stated concentrations of APAP for 24 h. (**b**) Representative immunofluorescence microscopy (IFM) images of embryos cultured with media (control) or media with the stated concentrations of APAP for 24 h. Upper panels: Differential interference contrast (DIC) analysis of the embryos. Middle panels: Primitive endoderm cells stained by anti-GATA4 (magenta) and the nuclei stained using DAPI (blue). Lower panels: trophectoderm cells (red) stained by anti-CDX2 antibody and inner cell mass (ICM) cells stained by anti-OCT3/4 antibody (green). (**c**) Quantification of the total cell numbers based on IFM analysis of embryos cultured for 24 h in media (control; n = 26) or media with APAP at the stated concentrations (100 µM: n = 14, 150 µM: n = 21, 200 µM: n = 26). (**d**) Quantification of cell number of the ICM based on IFM analysis of embryos cultured for 24 h in media (control; n = 15) or media with APAP at the stated concentrations (100 µM: n = 9, 150 µM: n = 14, 200 µM: n = 19). (**e**) Representative IFM images of embryos cultured in media (control) or 200 µM APAP for 24 h. Upper panels: Microtubule structures stained by anti-tubulin antibody (red) and nuclei stained with DAPI (blue). Lower panel: F-actin stained by Phalloidin (green) and microtubule structures stained by anti-tubulin antibody (red). The embryonic day in the parenthesis (E4.5) corresponds to their embryonic age at the end of the given exposure time. Statistical significance was tested with ordinary one-way ANOVA ($F(3, 83) = 0.1426$ (c); $F(3, 53) = 5.996$ (d)) followed by Dunnett's multiple comparison *post hoc* test (against control). Data points are represented as mean±SEM. ***$P < 0.001$.

Discussion

The initial days during PID are arguably the most critical phase in human development (Jarvis, 2016a,b; Muter *et al.*, 2023). It is estimated that 10–40% of early embryos are lost before or at the time of implantation (Roberts and Lowe, 1975; Wilcox *et al.*, 1988, 1999; Zinaman *et al.*, 1996; Wang *et al.*, 2003; Jarvis, 2016a,b; Foo *et al.*, 2020; Muter *et al.*, 2023). In this study, we show that APAP might disrupt embryonic development during this sensitive period of life by inhibiting the cell cycle.

In the search for the exact mechanism, we cannot dismiss potential effects on pharmaceutical targets such as PTGS1, PTGS2, and CB1 in the presented data. While this limitation is significant for our mouse and human data, the data from *S. pombe* suggest that inhibition of RNR is a plausible cause of the cycle effects, as suggested by others (Hongslo *et al.*, 1990). Accordingly, we consistently observed inhibition of DNA synthesis in *in vitro* models and in human embryos. Interestingly, a comparable effect has previously been identified *in vivo* 1 h after an oral dose of 125 mg/kg in a rodent study (Lister and McLean, 1997). Another limitation to be mentioned is the role of NAPQI in relation to the inhibition of DNA synthesis. However, the direct impact on the cell cycle without effects on cell viability, e.g. in HEK293 and hESCs, suggests that NAPQI levels were low and rapidly detoxified. Supporting this is the fact that NAPQI was not detected in the media after 72 h of exposure to 500 µM APAP *in vitro*. The low levels of S-CH_3-APAP-S detected could suggest that a small amount of APAP had been metabolized to NAPQI, followed by conjugation to glutathione before transformation to cysteine and mercapturate conjugates via the mercapturate pathway, and finally metabolized to S-CH_3-APAP-S via a thiomethyl shunt (David *et al.*, 2021). As NAPQI is rapidly conjugated to glutathione, and considering that the levels of S-CH_3-APAP-S detected were very low compared to APAP, it is unlikely that the cells were affected by NAPQI. Moreover, a previous study has found no reduction in glutathione levels in PID embryos after APAP exposure (375–1500 µM) *ex vivo* and in ovaries and PID embryos (800 and 1430 mg/kg/day) *in vivo* (Laub *et al.*, 2000). Together with our *in vitro* data, this strongly suggests that the observed effects on the cell cycle were not dependent on NAPQI activity. Instead, our modeling suggests a direct interaction with a critical tyrosyl free radical in the cofactor site of RNR, as also suggested previously (Hongslo *et al.*, 1990). Fascinatingly, a similar inhibition in the formation of a tyrosyl free radical in prostaglandin H2 synthase 1

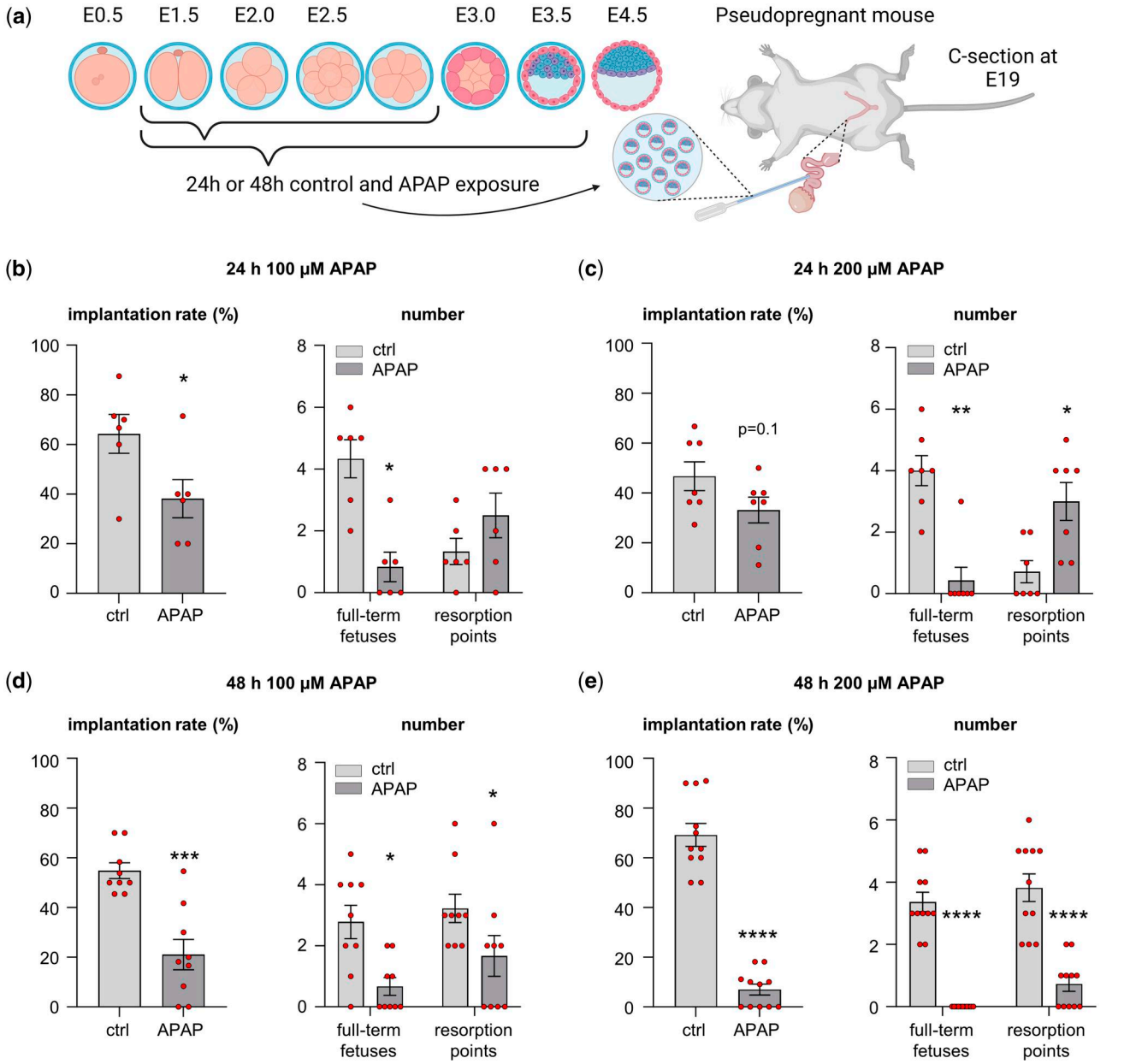

Figure 3. Transfers of cleavage-stage mouse C57BL/6 embryos exposed to paracetamol (N-acetyl-para-aminophenol (APAP)) for 24 or 48 h result in reduced pregnancy outcomes. (**a**) Schematic illustration that shows transfer of control and APAP-exposed blastocyst-stage embryos to each uterine horn of pseudo-pregnant recipients, respectively, as well as the timing and duration of the APAP exposure. (**b**) Implantation rate and number of full-term fetuses and resorption points for 24 h (100 µM, n = 6) APAP/control exposed E1.5 embryos. (**c**) Implantation rate and number of full-term fetuses and resorption points for 24 h (200 µM, n = 7) APAP/control exposed E1.5 embryos. (**d**) Implantation rate and number of full-term fetuses and resorption points for 48 h (100 µM, n = 9) APAP/control exposed E1.5 embryos. (**e**) Implantation rate and number of full-term fetuses and resorption points for 48 h (200 µM, n = 11) APAP/control exposed E1.5 embryos. Statistical significance of the implantation rate was tested with a two-tailed Student's unpaired *t*-test ($t = 2.385$, df = 10 (b^{left}); $t = 1.754$, df = 12 (c^{left}); $t = 4.894$, df = 16 (d^{left}); $t = 12.22$, df = 20 (e^{left})). A Mann–Whitney compare ranks test followed by Holm–Šídák multiple comparison *post hoc* test was used to test for statistical significance of full-term fetuses and resorption points (b^{right}, c^{right}, d^{right}, e^{right}). Data points are represented as mean±SEM. *$P \leq 0.05$; **$P < 0.01$; ***$P < 0.001$; ****$P < 0.0001$.

and 2 is the likely mechanism by which APAP mediates its analgesic and anti-pyretic effects (Aronoff *et al.*, 2006).

In the human uterus, we found an average concentration of 124.5 µM after a standard oral pharmaceutical dose of 1 g, which is similar to the average of 120 µM found in plasma after a similar oral dose (Langford *et al.*, 2016; Rehfeld *et al.*, 2022), suggesting that APAP is readily transferred from the blood to the intrauterine environment. It is intrinsically difficult to investigate dose–response relationship during PID *in utero*. We therefore used a mouse model with *ex vivo* dose–response exposure followed by transfer to recipient pseudo-pregnant dams to understand the effects on subsequent development. Using this model, we observed a time and concentration-dependent effect on growth and the rate of blastocyst formation of embryos exposed to concentrations exceeding 25 µM APAP *ex vivo*. Importantly, a comparable inhibition of mouse PID development has been observed previously with higher APAP concentrations of 375–1500 µM (Laub *et al.*, 2000). After the transfer of embryos exposed to 100 and 200 µM to recipient pseudo-pregnant dams, the number of implantations and full-term fetuses was reduced in APAP-

exposed embryos as compared to control embryos in a dose- and exposure-dependent manner. These findings suggest that the disruption of PID caused by APAP at human physiological relevant concentrations for 24 or 48 h reduces the likelihood of full-term development in the mouse.

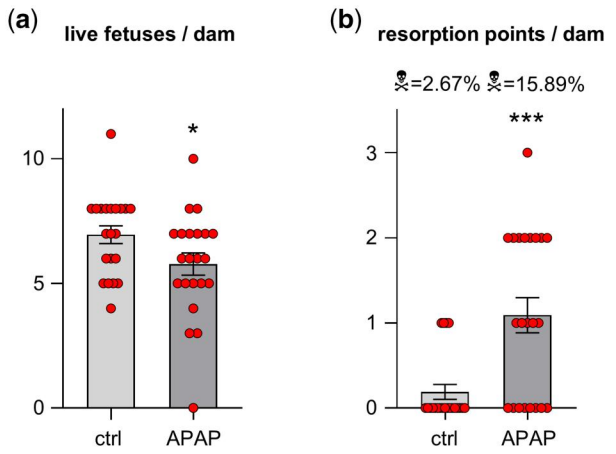

Figure 4. In vivo exposure to paracetamol (N-acetyl-para-aminophenol (APAP)) during C57Bl/6 mouse embryonic development results in reduced pregnancy outcomes. (**a**) Number of live fetuses per dam, (ctrl: n = 21, APAP: n = 22). (**b**) Number of resorption points per dam (ctrl: n = 21, APAP: n = 22). Statistical significance was tested with a two-tailed Student's unpaired *t*-test ($t = 2.057$, df = 41 (a)), or a Mann–Whitney compare ranks test (b). Data points are represented as mean ± SEM. *$P < 0.05$; ***$P < 0.001$.

Both mouse and human cleavage-stage embryos were more sensitive to APAP than the later blastocyst-stage embryos, with direct embryonic fatality at a concentration of 200 µM. Interestingly, in mice, we also observed an effect on the ICM of blastocyst-stage embryos when exposed to 200 µM. A similar impact was identified in human blastocyst-stage embryos with 100 µM after 6 h, with a comparable trend at 200 µM. These changes in morphology were associated with a decrease in DNA synthesis in OCT3/4 expressing ICM cells. Together, this suggests not only that the pluripotent ICM shares sensitivity to APAP with the blastomeres of cleavage-stage embryos, but also that even a few hours of exposure are sufficient to induce adverse effects on PID at concentrations similar to or lower than those found in the uterus of women (maximal concentration measured was 291 µM).

In our mouse pregnancy model, we observed effects on both the number of offspring and resorption points after a bulk gavage with a subtoxic dose of 200 mg/kg/day during PID and the days after implantation. It is a limitation of the model that the dose was not split into multiple boli (e.g. administration every 6 h), resembling use during human pregnancy. Such multiple exposures would have provided a sustained exposure but would simultaneously also have induced unwanted stress among the dams. Moreover, a previous study has shown that the administration of a bolus gavage dose of 200 mg/kg resulted in an average serum concentration of 37.5 µM APAP in mice 2 h after administration (Fleischmann *et al.*, 2017). Assuming that the concentrations of APAP in the reproductive tract of mice are comparable to serum concentrations, the gavage dose of 200 mg/kg resulted in concentrations that were comparable to the dose of 50 µM in our *ex vivo* experiments (Fig. 1) and were in the lower range of what was

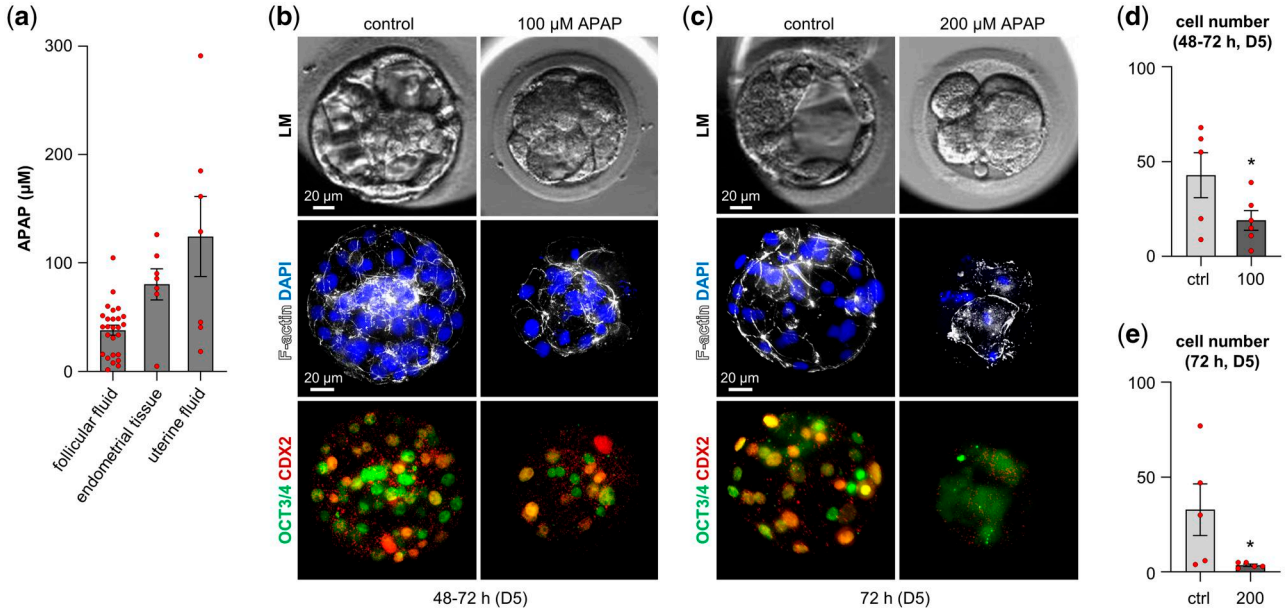

Figure 5. Paracetamol (N-acetyl-para-aminophenol (APAP)) reaches the human intrauterine environment and disrupts human cleavage-stage embryo development. (**a**) APAP concentrations in follicular fluid (n = 26), endometrial tissue (n = 7), and uterine fluid (n = 7) 1 h after a 1 g oral dose of APAP. (**b**) Representative embryoscope time-lapse and immunofluorescence microscopy (IFM) images of embryos cultured for 48–72 h in media (control) or media with 100 µM APAP. Upper panels: Embryoscope image of embryos (LM). Middle panels: F-actin stained by Phalloidin (white) and the nuclei stained using DAPI (blue). Lower panels: trophectoderm (TE) cells (red) stained by anti-CDX2 antibody and inner cell mass (ICM) cells stained by anti-OCT3/4 antibody (green). (**c**) Representative embryoscope time-lapse and IFM images of embryos cultured for 72 h in media (control) or media with 200 µM APAP. Upper panels: Embryoscope image of embryos (LM). Middle panels: F-actin stained by Phalloidin (white) and the nuclei stained by DAPI (blue). Lower panels: TE cells (red) stained by anti-CDX2 antibody and ICM cells stained by anti-OCT3/4 antibody (green). (**d**) Quantification of cell numbers based on IFM analysis of embryos cultured for 48–72 h in media (control, n = 5) or media with APAP 100 µM (n = 6). (**e**) Quantification of cell numbers based on embryoscope- and IFM analysis of embryos cultured for 72 h in media (control, n = 5) or media with APAP 100 µM (n = 5). The embryonic day in the parenthesis (D5) corresponds to their embryonic age at the end of the given exposure time. Statistical significance was tested with a Student's one-tailed unpaired *t*-test ($t = 1.961$, df = 9 (d); $t = 2.142$, df = 8 (e)). Data points are represented as mean ± SEM. *$P < 0.05$. For embryoscope time-lapse videos, see Videos 1 and 2.

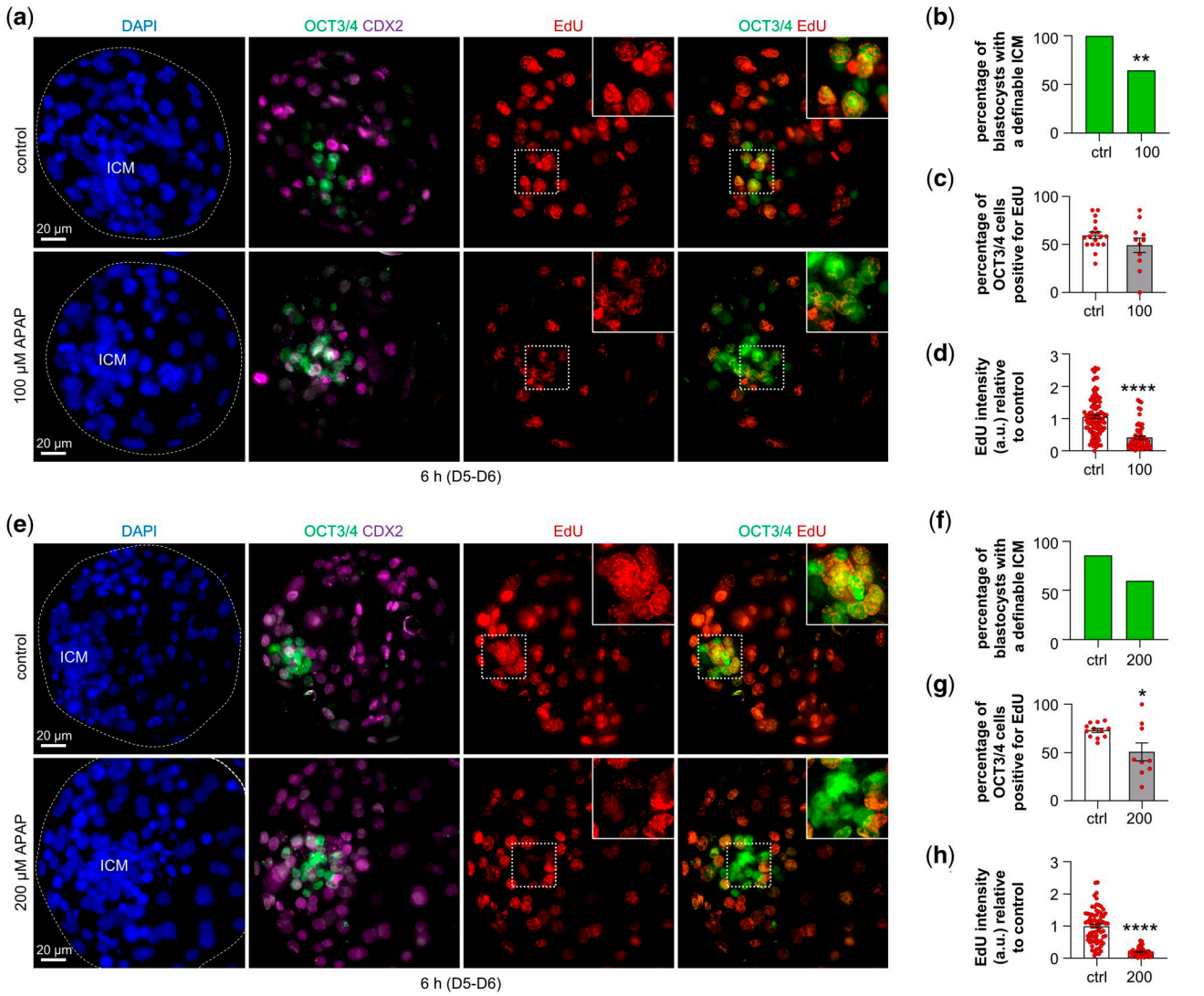

Figure 6. Paracetamol (N-acetyl-para-aminophenol (APAP)) disrupts human blastocyst-stage development and affects DNA synthesis. (**a**) Representative immunofluorescence microscopy (IFM) pictures of embryos cultured in media (control) or media with 100 µM APAP for 6 h and with EdU (red) for the final 3 h. The trophectoderm (TE) cells (magenta) were stained by anti-CDX2 antibody, inner cell mass (ICM) cells stained by anti-OCT3/4 antibody (green), and the nuclei stained with DAPI (blue). (**b**) Percentage of embryos with a definable ICM based on the IFM analysis (control; n = 18, 100 µm APAP; n = 18). (**c**) Percentage of OCT3/4 cells positive for 5-ethynyl-2′-deoxyuridine (EdU) quantified based on the IFM analysis (control; n = 18, APAP; n = 11). (**d**) Quantification of the EdU fluorescence intensity from the OCT3/4 cells positive for EdU (control; n = 108 (108 cells from 18 blastocysts), APAP; n = 60 (60 cells from 11 blastocysts)). (**e**) As in (a) with control or 200 µM APAP. (**f**) As in (b) (control; n = 14, 200 µM APAP; n = 15). (**g**) As in (c) (control; n = 12, 200 µM APAP; n = 9). (**h**) As in (d) (control; n = 71 (71 cells from 11 blastocysts), 200 µM APAP; n = 37 (37 cells from nine blastocysts)). The embryonic day in the parenthesis (D5–D6) corresponds to their embryonic age at the end of the given exposure time. Statistical significance was on the percentage of embryos with a definable ICM tested with a Fisher's exact test. Statistical significance was, for the percentage of OCT3/4 cells positive for EdU and EdU fluorescence intensity from the OCT3/4 cells positive for EdU tested, with a two-tailed Student's unpaired *t*-test ($t = 1.428$, $df = 27$ (c); $t = 7.453$, $df = 166$ (d); $t = 2.673$, $df = 19$ (g); $t = 9.031$, $df = 106$ (h)). Data points are represented as mean ± SEM. $^*P < 0.05$; $^{**}P < 0.01$; $^{****}P < 0.0001$.

observed in human uterine fluid (Fig. 5). An important limitation of the *in vivo* experiment is therefore that a higher concentration than 200 mg/kg of APAP should have been used to reach comparable doses to what we found in the human intrauterine environment. However, increasing the doses used in the mouse model above 200 mg/kg/day for the pregnant dams would have increased the risk of toxicological effects, such as liver toxicity, potentially resulting in fetal loss not directly associated with the direct effects on the embryos. Accordingly, a comparable study found a similar trend of increased numbers of resorptions and decreased numbers of fetuses in APAP-treated dams using a dose of 1430 mg/kg/day, with the major caveat that the higher dose resulted in 25% of dams dying during the study (Laub *et al.*, 2000). Thus, a critical limitation of our pregnancy model was that the commonly used 12.33× dose translation between mice and humans in toxicological studies (Reagan-Shaw *et al.*, 2008) could not be applied due to the toxic effects of APAP on the liver. As this translation factor is based on major differences between mice and humans in biological parameters, such as oxygen utilization, caloric expenditure, basal metabolism, blood volume, circulating plasma proteins, and renal function (Reagan-Shaw *et al.*, 2008), effects on development might have been even more prevalent if higher doses could have been applied. Nevertheless, with a maximal human dose of 50 mg/kg/day, the 4× dose used here resulted in significant effects on number of live fetuses and miscarriages, well below the safety margin of 12.33× (Reagan-Shaw *et al.*, 2008).

In both mice and humans, implantation is dependent on a precisely timed interaction between the developing embryo and the hormonally primed endometrium. Studies in human have shown that successful implantation requires embryos to progress to the blastocyst stage and undergo timely hatching (Wilcox *et al.*, 1999). Delayed development leads to asynchrony between the developing embryo and the endometrium, thereby increasing the risk of implantation failure or miscarriage (Wilcox *et al.*, 1999). Moreover, ICM quality, defined by cell number and morphology, has been identified as the most significant predictor of live birth (Ai *et al.*, 2021). Based on the present data, we therefore suggest that APAP (depending on timing, duration, and concentration) might disrupt early development in three different scenarios: (i) *direct embryonic fatality* at higher doses, (ii) *failed implantation* due to asynchrony of the embryo and endometrium by delayed PID, and (iii) *miscarriage* after implantation due to disruption of PID *in situ*, e.g. reduced cell number in ICM.

APAP has long been considered a safe option for the treatment of pain and fever during pregnancy by regulatory bodies when used as directed (Food and Drug Administration, 2015; European Medicines Agency, 2019). Moreover, several studies from Europe have shown APAP exposure from the environment (Modick *et al.*, 2014; Nielsen *et al.*, 2015; Bornehag *et al.*, 2018), emphasizing its status not only as one of the most widely used pharmaceuticals globally but also as a significant environmental pollutant (Modick *et al.*, 2014; Kristensen *et al.*, 2016; Wilkinson *et al.*, 2022). The inherent challenges in investigating human PID (Wilcox *et al.*, 1999; Jarvis, 2016a,b) are a probable reason for the lack of previous studies identifying a link to APAP. Infertility affects 12.6–17.5% of reproductive-aged couples worldwide (Njagi *et al.*, 2023). As early embryonic fatality or failure of implantation is often interpreted as subfertility by health professionals (Wang *et al.*, 2003; Jarvis, 2016a,b), our data suggest that embryonic loss induced by xenobiotic chemicals as APAP could be an unrecognized contributor to the increasing infertility rates worldwide.

Among the limitations of the present study has also been the challenge of obtaining a large number of human cleavage-stage embryos. Our translational approach, demonstrating reproducibility across multiple model systems, partially mitigates this limitation. For instance, the recapitulation of cell cycle effects, as also observed in other studies in, e.g. a cancer cell line (Wiger *et al.*, 1997), from yeast to mouse preclinical models and human embryos, provides critical support for the disruptive effect of APAP. Further studies are now warranted to validate these findings. As the present study is experimental, such studies should include investigating APAP use among fertile healthy women and exploring the potential link to pregnancy loss in prospective cohorts to further support the clinical relevance of the observations. Given that cell division is fundamental to all development, additional research is also necessary to understand how environmentally induced cell cycle inhibition might impact other developmental processes, such as gonadal and brain differentiation.

Finally, it is important to note that APAP was introduced for medical use as an antipyretic/analgesic in the late 19th century (Przybyła *et al.*, 2021), prior to the establishment of regulatory bodies such as the US Federal Food and Drug Administration (FDA) (Borchers *et al.*, 2007). Additionally, ethical standards set by the FDA and the European Medicines Agency prohibit the inclusion of pregnant women or those trying to conceive in studies where harm to the offspring can be plausibly inferred (Mastroianni *et al.*, 1994), as is the case with prenatal exposure to APAP. As a result, translational studies, such as the present study, covering animal and human endpoints are of critical importance for understanding the potential effects of APAP use during pregnancy and for informing the ongoing debate about the safety of APAP (Bauer *et al.*, 2021).

Supplementary data

Supplementary data are available at *Human Reproduction* online.

Data availability

The data underlying this article are available within the article and in its online supplementary material. Should additional data be of interest, it will be shared upon reasonable request to the corresponding author.

Acknowledgements

We acknowledge and thank Dr Gavin Jarvis for helpful discussions concerning estimates of early pregnancy loss.

Authors' roles

D.M.K., B.S.N., K.K., and M.R.P. conceived and designed the study. D.M.K., B.S.N., M.R.P, J.M.-G., C.H., H.K.M., H.F., C.R., E.M.J., P.S., S. L.T.C., N.R.J., J.K., A.H.-S., M.H., P.A.P., A.J., A.P., S.Z., J.E., A.D., A. Z., and S.T.C. performed experiments. D.M.K., B.S.N., M.R.P., K.B. P., S.L., J.E., F.L., and A.Z. coordinated the surplus human embryo donations. D.M.K., B.S.N., M.R.P., S.T.C., and A.D. analyzed and interpreted the data. Drafting the article was performed by D.M. K., B.S.N., and M.R.P. All authors have read and approved the final version of this manuscript.

Funding

D.M.K. was supported by the Lundbeck Foundation (R324-2019-1881) to perform the study. Authors P.S. and H.K.M. are part of the Novo Nordisk Foundation Center for Stem Cell Medicine (reNEW; NNF21CC0073729). H.K.M. is the recipient of a fellowship from the Novo Nordisk Foundation as part of the Copenhagen Bioscience PhD Program, supported through grant NNF19SA0035442. M.H and A.D. are part of the National French Research Infrastructure France Exposome and have received funding from the European Regional Development Fund and Britanny Region (Contrat Plan Etat Region, project Exposome, AIDEN 106201) for the Bruker timsTOF Pro 2 instrument used in the study.

Conflict of interest

Authors declare no competing interests.

References

Abramson J, Adler J, Dunger J, Evans R, Green T, Pritzel A, Ronneberger O, Willmore L, Ballard AJ, Bambrick J *et al.* Accurate structure prediction of biomolecular interactions with AlphaFold 3. *Nature* 2024;**630**:493–500.

Ai J, Jin L, Zheng Y, Yang P, Huang B, Dong X. The morphology of inner cell mass is the strongest predictor of live birth after a frozen-thawed single embryo transfer. *Front Endocrinol (Lausanne)* 2021;**12**:621221.

Ameri J, Borup R, Prawiro C, Ramond C, Schachter KA, Scharfmann R, Semb H. Efficient generation of glucose-responsive beta cells

from isolated GP2+ human pancreatic progenitors. *Cell Rep* 2017; **19**:36–49.

Aronoff DM, Oates JA, Boutaud O. New insights into the mechanism of action of acetaminophen: its clinical pharmacologic characteristics reflect its inhibition of the two prostaglandin H2 synthases. *Clin Pharmacol Ther* 2006;**79**:9–19.

Artacho-Cordón F, Arrebola JP, Nielsen O, Hernández P, Skakkebaek NE, Fernández MF, Andersson AM, Olea N, Frederiksen H. Assumed non-persistent environmental chemicals in human adipose tissue; matrix stability and correlation with levels measured in urine and serum. *Environ Res* 2017;**156**:120–127.

Bauer AZ, Swan SH, Kriebel D, Liew Z, Taylor HS, Bornehag CG, Andrade AM, Olsen J, Jensen RH, Mitchell RT *et al.* Paracetamol use during pregnancy–a call for precautionary action. *Nat Rev Endocrinol* 2021;**17**:757–766.

Bertoldi AD, Rifas-Shiman SL, Boing AC, Silva da Dal Pizzol T, Miranda VIA, Silveira MPT, Freitas Silveira M, Domingues MR, Santos IS, Bassani DG *et al.* Associations of acetaminophen use during pregnancy and the first year of life with neurodevelopment in early childhood. *Paediatr Perinat Epidemiol* 2020; **34**:267–277.

Borchers AT, Hagie F, Keen CL, Gershwin ME. The history and contemporary challenges of the US Food and Drug Administration. *Clin Ther* 2007;**29**:1–16.

Bornehag CG, Reichenberg A, Hallerback MU, Wikstrom S, Koch HM, Jonsson BA, Swan SH. Prenatal exposure to acetaminophen and children's language development at 30 months. *Eur Psychiatry* 2018;**51**:98–103.

Brown S. Miscarriage and its associations. *Semin Reprod Med* 2008; **26**:391–400.

Brunborg G, Holme JA, Hongslo JK. Inhibitory effects of paracetamol of DNA repair in mammalian cells. *Mutat Res* 1995;**342**:157–170.

Callahan BJ, DiGiulio DB, Aliaga Goltsman DS, Sun CL, Costello EK, Jeganathan P, Biggio JR, Wong RJ, Druzin ML, Shaw GM *et al.* Replication and refinement of a vaginal microbial signature of preterm birth in two racially distinct cohorts of US women. *Proc Natl Acad Sci USA* 2017;**114**:9966–9971.

Corso G, Stärk H, Jing B, Barzilay R, Jaakkola T. DiffDock: Diffusion Steps, Twists, and Turns for Molecular Docking. arXiv. https://doi.org/10.48550/arXiv.2210.01776, 2022, preprint: not peer reviewed.

David A, Chaker J, Léger T, Al-Salhi R, Dalgaard MD, Styrishave B, Bury D, Koch HM, Jégou B, Kristensen DM. Acetaminophen metabolism revisited using non-targeted analyses: implications for human biomonitoring. *Environ Int* 2021;**149**:106388.

Elovitz MA, Gajer P, Riis V, Brown AG, Humphrys MS, Holm JB, Ravel J. Cervicovaginal microbiota and local immune response modulate the risk of spontaneous preterm delivery. *Nat Commun* 2019; **10**:1305.

Ernstsen C, Christensen SL, Olesen J, Kristensen DM. No additive effect of combining sumatriptan and olcegepant in the GTN mouse model of migraine. *Cephalalgia* 2021;**41**:329–339.

European Medicines Agency. *PRAC recommendations on signals: adopted at the 12–15 March 2019 PRAC meeting*. 2019,31. https://www.ema.europa.eu/en/documents/prac-recommendation/prac-recommendations-signals-adopted-12-15-march-2019-prac-meeting_en.pdf (28 May 2025, date last accessed).

Food and Drug Administration. FDA Drug Safety Communications: FDA has reviewed possible risks of pain medicine use during pregnancy. 2015. https://www.fda.gov/media/90209/download (28 May 2025, date last accessed).

Fettweis JM, Serrano MG, Brooks JP, Edwards DJ, Girerd PH, Parikh HI, Huang B, Arodz TJ, Edupuganti L, Glascock AL *et al.* The vaginal microbiome and preterm birth. *Nat Med* 2019;**25**:1012–1021.

Fleck O, Vejrup-Hansen R, Watson A, Carr AM, Nielsen O, Holmberg C. Spd1 accumulation causes genome instability independently of ribonucleotide reductase activity but functions to protect the genome when deoxynucleotide pools are elevated. *J Cell Sci* 2013; **126**:4985–4994.

Fleischmann T, Arras M, Sauer M, Saleh L, Rülicke T, Jirkof P. Voluntary intake of paracetamol-enriched drinking water and its influence on the success of embryo transfer in mice. *Res Vet Sci* 2017;**111**:85–92.

Foo L, Johnson S, Marriott L, Bourne T, Bennett P, Lees C. Peri-implantation urinary hormone monitoring distinguishes between types of first-trimester spontaneous pregnancy loss. *Paediatr Perinat Epidemiol* 2020;**34**:495–503.

Gardner DK, Lane M, Stevens J, Schlenker T, Schoolcraft WB. Blastocyst score affects implantation and pregnancy outcome: towards a single blastocyst transfer. *Fertil Steril* 2000; **73**:1155–1158.

Gorrochategui E, Le Vee M, Selmi H, Gérard A, Chaker J, Krais AM, Lindh C, Fardel O, Chevrier C, Le Cann P *et al.* High-resolution mass spectrometry identifies delayed biomarkers for improved precision in acetaminophen/paracetamol human biomonitoring. *Environ Int* 2023;**181**:108299.

Holm JB, Mazaud-Guittot S, Danneskiold-Samsøe NB, Chalmey C, Jensen B, Nørregård MM, Hansen CH, Styrishave B, Svingen T, Vinggaard AM *et al.* Intrauterine exposure to paracetamol and aniline impairs female reproductive development by reducing follicle reserves and fertility. *Toxicol Sci* 2016;**150**:178–189.

Hongslo JK, Bjørge C, Schwarze PE, Brøgger A, Mann G, Thelander L, Holme JA. Paracetamol inhibits replicative DNA synthesis and induces sister chromatid exchange and chromosomal aberrations by inhibition of ribonucleotide reductase. *Mutagenesis* 1990; **5**:475–480.

Iakovidou MC, Kolibianakis E, Zepiridis L, Venetis C. The role of endometrial scratching prior to in vitro fertilization: an updated systematic review and meta-analysis. *Reprod Biol Endocrinol* 2023; **21**:89.

ICH. *ICH Harmonized Tripartite Guideline: Validation of Analytical Procedures: Text and Methodology Q2(R1)*. Geneva, Switzerland: International Council for Harmonization of Technical Requirements for Pharmaceuticals for Human Use (ICH), 2005,1–17. https://database.ich.org/sites/default/files/Q2%28R1%29%20Guideline.pdf (28 May 2025, date last accessed).

Iwasa T, Kuwahara A, Takeshita T, Taniguchi Y, Mikami M, Irahara M. Preimplantation genetic testing for aneuploidy and chromosomal structural rearrangement: a summary of a nationwide study by the Japan Society of Obstetrics and Gynecology. *Reprod Med Biol* 2023;**22**:e12518.

Jarvis GE. Estimating limits for natural human embryo mortality. *F1000Res* 2016a;**5**:2083.

Jarvis GE. Early embryo mortality in natural human reproduction: what the data say. *F1000Res* 2016b;**5**:2765.

Johnson M. Manipulating the mouse embryo: a laboratory manual. *Trends Genet* 1986;**2**:298.

Kiprilov EN, Awan A, Desprat R, Velho M, Clement CA, Byskov AG, Andersen CY, Satir P, Bouhassira EE, Christensen ST *et al.* Human embryonic stem cells in culture possess primary cilia with hedgehog signaling machinery. *J Cell Biol* 2008;**180**:897–904.

Kristensen DM, Mazaud-Guittot S, Gaudriault P, Lesné L, Serrano T, Main KM, Jégou B. Analgesic use-prevalence, biomonitoring and endocrine and reproductive effects. *Nat Rev Endocrinol* 2016; **12**:381–393.

Langford RA, Hogg M, Bjorksten AR, Williams DL, Leslie K, Jamsen K, Kirkpatrick C. Comparative plasma and cerebrospinal fluid

pharmacokinetics of paracetamol after intravenous and oral administration. *Anesth Analg* 2016;**123**:610–615.

Laub DN, Elmagbari NO, Elmagbari NM, Hausburg MA, Gardiner CS. Effects of acetaminophen on preimplantation embryo glutathione concentration and development in vivo and in vitro. *Toxicol Sci* 2000;**56**:150–155.

Lister CF, McLean AEM. Inhibition of DNA synthesis by paracetamol in different tissues of the rat in vivo. *Toxicology* 1997;**116**:49–57.

Luz AL, Tokar EJ. Pluripotent stem cells in developmental toxicity testing: a review of methodological advances. *Toxicol Sci* 2018;**165**:31–39.

Masarwa R, Levine H, Gorelik E, Reif S, Perlman A, Matok I. Prenatal exposure to acetaminophen and risk for attention deficit hyperactivity disorder and autistic spectrum disorder: a systematic review, meta-analysis, and meta-regression analysis of cohort studies. *Am J Epidemiol* 2018;**187**:1817–1827.

Mastroianni AC, Faden R, Federman D. Women and health research: a report from the Institute of Medicine. *Kennedy Inst Ethics J* 1994;**4**:55–62.

Modick H, Weiss T, Dierkes G, Brüning T, Koch HM. Ubiquitous presence of paracetamol in human urine: sources and implications. *Reproduction* 2014;**147**:R105–R117.

Muter J, Lynch VJ, McCoy RC, Brosens JJ. Human embryo implantation. *Development* 2023;**150**:dev201507.

Niakan KK, Eggan K. Analysis of human embryos from zygote to blastocyst reveals distinct gene expression patterns relative to the mouse. *Dev Biol* 2013;**375**:54–64.

Nielsen JKS, Modick H, Mørck TA, Jensen JF, Nielsen F, Koch HM, Knudsen LE. N-acetyl-4-aminophenol (paracetamol) in urine samples of 6-11-year-old Danish school children and their mothers. *Int J Hyg Environ Health* 2015;**218**:28–33.

Niwa H, Toyooka Y, Shimosato D, Strumpf D, Takahashi K, Yagi R, Rossant J. Interaction between Oct3/4 and CDX2 determines trophectoderm differentiation. *Cell* 2005;**123**:917–929.

Njagi P, Groot W, Arsenijevic J, Dyer S, Mburu G, Kiarie J. Financial costs of assisted reproductive technology for patients in low-and middle-income countries: a systematic review. *Hum Reprod Open* 2023;**2023**:hoad007.

Przybyła GW, Szychowski KA, Gmiński J. Paracetamol—an old drug with new mechanisms of action. *Clin Exp Pharmacol Physiol* 2021;**48**:3–19.

Reagan-Shaw S, Nihal M, Ahmad N. Dose translation from animal to human studies revisited. *FASEB J* 2008;**22**:659–661.

Regan L, Rai R. Epidemiology and the medical causes of miscarriage. *Baillieres Best Pract Res Clin Obstet Gynaecol* 2000;**14**:839–854.

Rehfeld A, Frederiksen H, Rasmussen RH, David A, Chaker J, Nielsen BS, Nielsen JE, Juul A, Skakkebæk NE, Kristensen DM. Human sperm cells can form paracetamol metabolite AM404 that directly interferes with sperm calcium signalling and function through a CatSper-dependent mechanism. *Hum Reprod* 2022;**37**:922–935.

Roberts CJ, Lowe CR. Where have all the conceptions gone? *Lancet* 1975;**305**:498–499.

Schmid FM, Schou KB, Vilhelm MJ, Holm MS, Breslin L, Farinelli P, Larsen LA, Andersen JS, Pedersen LB, Christensen ST. IFT20 modulates ciliary PDGFRα signaling by regulating the stability of Cbl E3 ubiquitin ligases. *J Cell Biol* 2018;**217**:151–161.

Schymanski EL, Jeon J, Gulde R, Fenner K, Ruff M, Singer HP, Hollender J. Identifying small molecules via high resolution mass spectrometry: communicating confidence. *Environ Sci Technol* 2014;**48**:2097–2098.

Serrano MG, Parikh HI, Brooks JP, Edwards DJ, Arodz TJ, Edupuganti L, Huang B, Girerd PH, Bokhari YA, Bradley SP *et al.* Racioethnic diversity in the dynamics of the vaginal microbiome during pregnancy. *Nat Med* 2019;**25**:1001–1011.

Servey J, Chang J. Over-the-counter medications in pregnancy. *Am Fam Physician* 2014;**90**:548–555.

Smarr MM, Kannan K, Chen Z, Kim S, Buck Louis GM. Male urinary paracetamol and semen quality. *Andrology* 2017;**5**:1082–1088.

Srikanth CV, Chakraborti AK, Bachhawat AK. Acetaminophen toxicity and resistance in the yeast *Saccharomyces cerevisiae*. *Microbiology (Reading)* 2005;**151**:99–111.

Stierand K, Maass PC, Rarey M. Molecular complexes at a glance: automated generation of two-dimensional complex diagrams. *Bioinformatics* 2006;**22**:1710–1716.

Van Hoogenhuijze NE, Kasius JC, Broekmans FJM, Bosteels J, Torrance HL. Endometrial scratching prior to IVF; does it help and for whom? A systematic review and meta-analysis. *Hum Reprod Open* 2019;**2019**:hoy025.

Wang X, Chen C, Wang L, Chen D, Guang W, French J, Xu X. Conception, early pregnancy loss, and time to clinical pregnancy: a population-based prospective study. *Fertil Steril* 2003;**79**:577–584.

Werler MM, Mitchell AA, Hernandez-Diaz S, Honein MA. Use of over-the-counter medications during pregnancy. *Am J Obstet Gynecol* 2005;**193**:771–777.

Wiger R, Finstad HS, Hongslo JK, Haug K, Holme JA. Paracetamol inhibits cell cycling and induces apoptosis in HL-60 cells. *Pharmacol Toxicol* 1997;**81**:285–293.

Wilcox AJ, Baird DD, Weinberg CR. Time of implantation of the conceptus and loss of pregnancy. *N Engl J Med* 1999;**340**:1796–1799.

Wilcox AJ, Weinberg CR, O'Connor JF, Baird DD, Schlatterer JP, Canfield RE, Armstrong EG, Nisula BC. Incidence of early loss of pregnancy. *N Engl J Med* 1988;**319**:189–194.

Wilkinson JL, Boxall ABA, Kolpin DW, Leung KMY, Lai RWS, Galban-Malag C, Adell AD, Mondon J, Metian M, Marchant RA *et al.* Pharmaceutical pollution of the world's rivers. *Proc Natl Acad Sci USA* 2022;**119**:e2113947119.

Wong FCK. Whole-mount immunofluorescence staining of early mouse embryos. *Methods Mol Biol* 2021;**2214**:143–155.

Wood V, Harris MA, McDowall MD, Rutherford K, Vaughan BW, Staines DM, Aslett M, Lock A, Bähler J, Kersey PJ *et al.* PomBase: a comprehensive online resource for fission yeast. *Nucleic Acids Res* 2012;**40**:D695–D699.

Yang Z, Liu J, Collins GS, Salem SA, Liu X, Lyle SS, Peck AC, Sills ES, Salem RD. Selection of single blastocysts for fresh transfer via standard morphology assessment alone and with array CGH for good prognosis IVF patients: results from a randomized pilot study. *Mol Cytogenet* 2012;**5**:24.

Zhao X, Georgieva B, Chabes A, Domkin V, Ippel JH, Schleucher J, Wijmenga S, Thelander L, Rothstein R. Mutational and structural analyses of the ribonucleotide reductase inhibitor sml1 define its rnr1 interaction domain whose inactivation allows suppression of mec1 and rad53 lethality. *Mol Cell Biol* 2000;**20**:9076–9083.

Zinaman MJ, Clegg ED, Brown CC, O'Connor J, Selevan SG. Estimates of human fertility and pregnancy loss. *Fertil Steril* 1996;**65**:503–509.

OXFORD
human reproduction
Human Reproduction, 2025, 1–1
https://doi.org/10.1093/humrep/deaf116
Supplementary Data

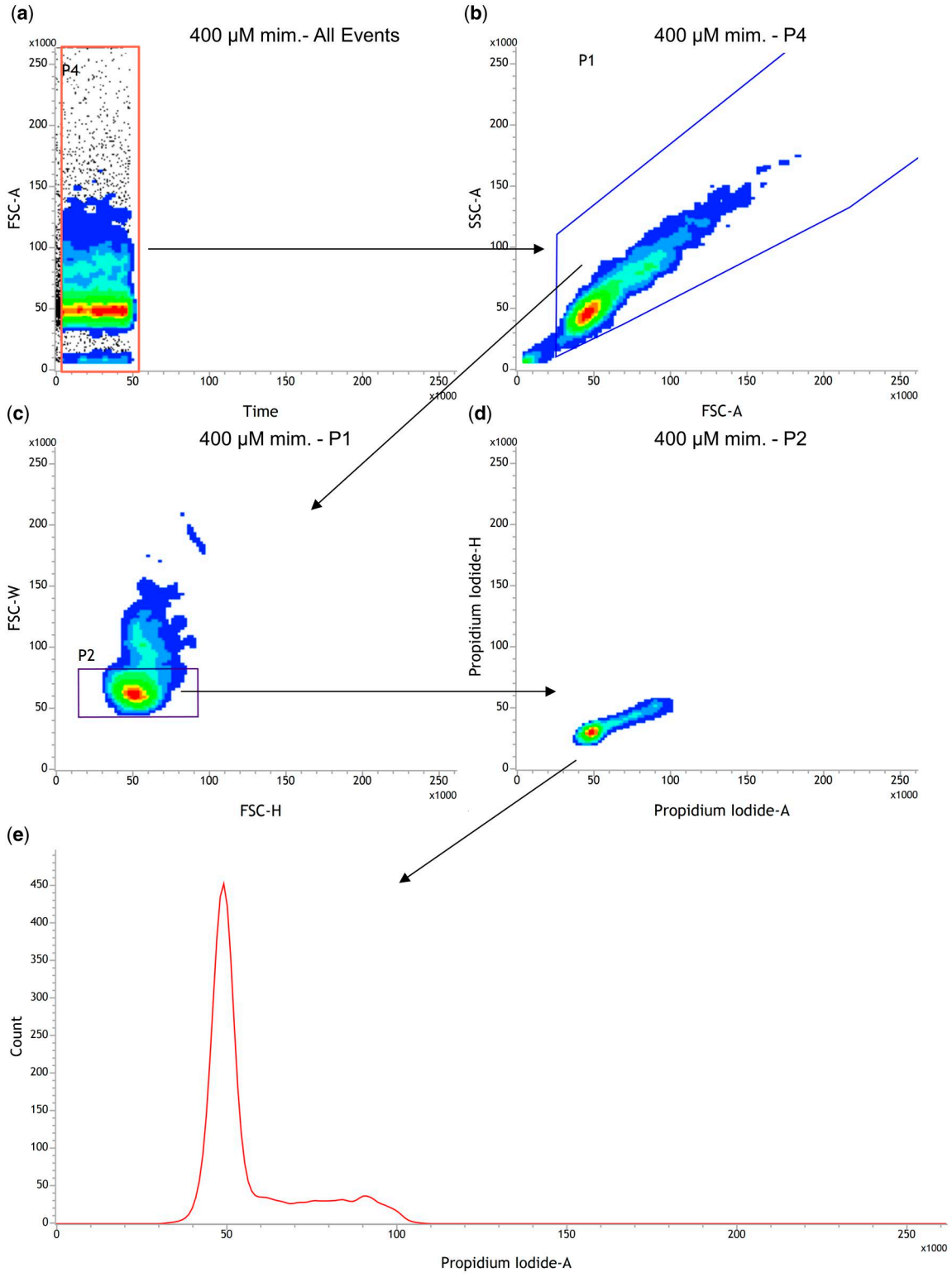

Supplementary Figure S1. Gating strategy exemplified by L-Mimosine arrest in the G1 phase before entry into the S phase using HEK293 cells. (**a**) Flow stability gating. (**b**) FSC-A and SSC-A were used to identify the intact cells and to exclude debris. (**c**) FSC-W and FSC-H were utilized to exclude doublets. (**d, e**) Single cells were gated using Propidium iodide-H and Propidium iodide-A to exclude outliers and subsequently applied to the propidium iodide histogram plot.

OXFORD
human reproduction
Human Reproduction, 2025, 1–1
https://doi.org/10.1093/humrep/deaf116
Supplementary Data

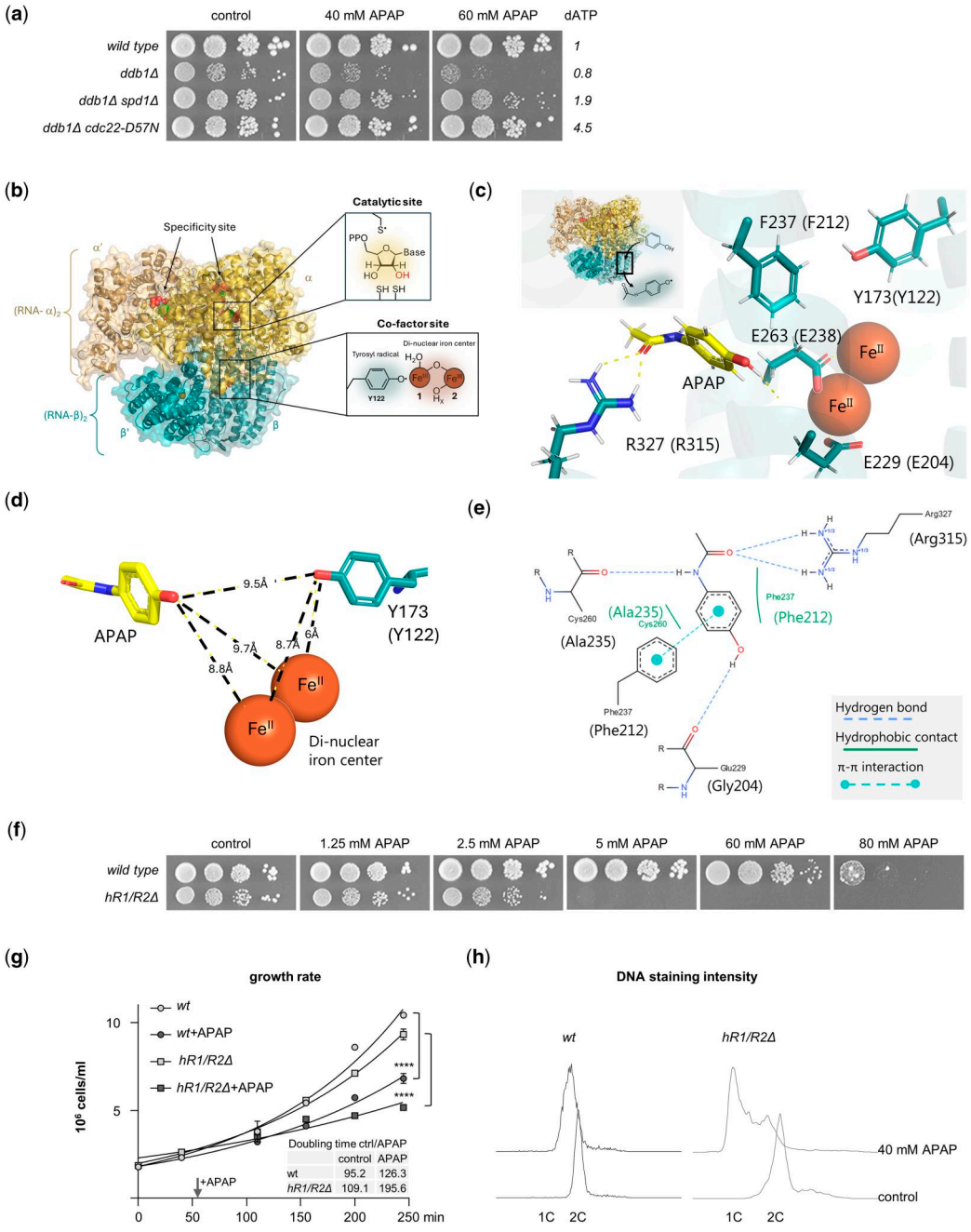

Supplementary Figure S2. Paracetamol (N-acetyl-para-aminophenol (APAP)) inhibits growth of yeast cells through ribonucleotide reductase (RNR). (**a**) Representative spot tests with 10-fold dilution series of the indicated strains plated onto agar without (DMSO, 1% (v/v)) and with APAP at the stated concentrations and allowed to grow at 32°C for 3 days before photography. Relative dATP concentration in the strains is inferred from (Fleck *et al.*, 2013) and indicated to the right (n = 3). (**b**) Structure of the holocomplex of *Escherichia coli* (*E. coli*) RNR (PDB 6W4X). Insert shows the location of the active site in the catalytic α subunit and the co-factor site in the β subunit. (**c**) Position and interaction of APAP in the β unit of ribonucleoside reductase (β-RNR) from *Schizosaccharomyces pombe* (*S. pombe*) (UniProt ID: P36603). The amino acid numbering refers to the *in silico* predicted structure of β-RNR from *S. pombe*. The numbers in parentheses are the equivalent residues in β-RNR from *E. coli*. (**d**) Interatomic distances between the hydroxy-group of docked APAP with tyrosine (Y173) and iron atoms in the cofactor site of β-RNR from *S. pombe*. APAP was located opposite to Y173 at a similar distance to the di-nuclear iron center. (**e**) 2D interaction diagrams illustrating the types of interactions that potentially can stabilize APAP in the co-factor site of β-RNR from *S. pombe*. (**f**) Serial plating as in (a), here with the WT strain and a strain relying on human RNR as indicated to the left (n = 3). (**g**) Growth rate in liquid culture with 1% (v/v) DMSO (control) or 40 mM APAP added at time point 55 min as indicated by arrow. Data points are represented as mean ± SD (n = 3). (**h**) Analysis of DNA content of the indicated strains exposed to 40 mM APAP or 1% (v/v) DMSO. Statistical significance (at 245 min of growth) was tested with two-way ANOVA (Interaction: F (1, 8) = 4.725; Strain: F (1, 8)=115.9; Treatment: F (1, 8)=927.7), followed by Šídák multiple comparison *post hoc* test. ****$P < 0.0001$.

OXFORD
human reproduction
Human Reproduction, 2025, 1–1
https://doi.org/10.1093/humrep/deaf116
Supplementary Data

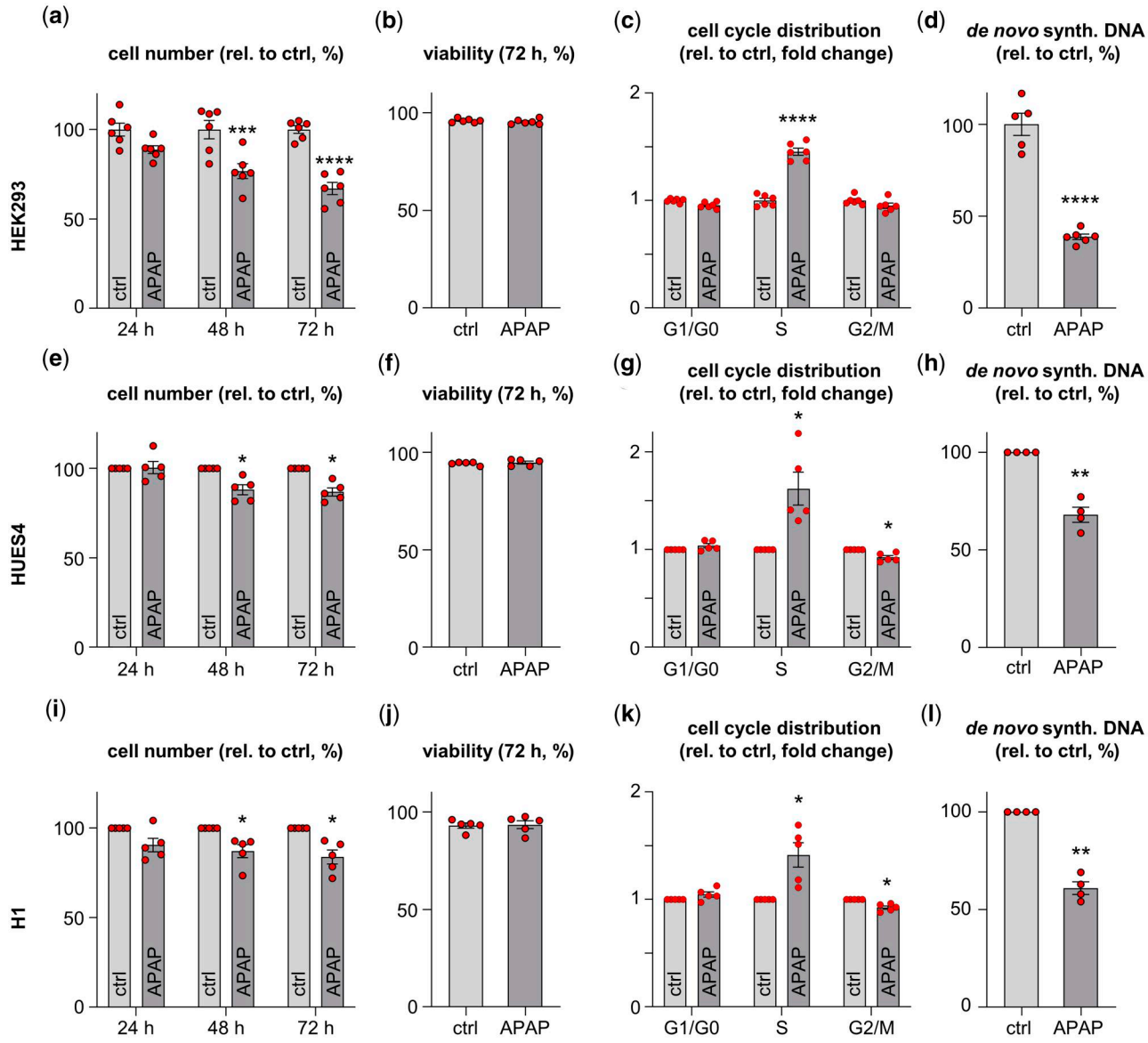

Supplementary Figure S3. Paracetamol (N-acetyl-para-aminophenol (APAP)) inhibits DNA synthesis, delays S phase transition, and reduces proliferation in human somatic and embryonic stem cells. (**a, b, e, f, i, j**) Cell count and viability percentage from 1 to 3 days of somatic HEK293 cells (500 µM, n = 6) and embryonic stem cells HUES4 (200 µM, n = 5) and H1 (200 µM, n = 5) exposed to control media (DMSO, 0.1% (v/v)) or media with APAP. Viability only shown for Day 3. (**c, g, k**) Propidium iodide-based cell cycle analysis by flow cytometry of HEK293 (500 µM, n = 6), HUES4 (200 µM, n = 5), and H1 (200 µM, n = 5) cells exposed to control media (DMSO, 0.1% (v/v)) or media with APAP. Data are after 48 h of exposure. (**d, h, l**) *de novo* DNA synthesis of control (DMSO, 0.1% (v/v)) or APAP exposed HEK293 (500 µM, ctrl: n = 5, APAP: n = 6), HUES4 (200 µM, n = 4), and H1 (200 µM, n = 4) cells using flow cytometry after 3 h of APAP exposure with EdU added for the final 2 h. Statistical significance was tested with two-way ANOVA (Interaction: F (2, 30)=4.627; Time: F (2, 30)=4.627; Treatment: F (1, 30)=58.68 (a), Interaction: F (2, 30)=96.16; Cell cycle phase: F (2, 30)=96.16; Treatment F (1, 30)= 50.30 (c)) followed by Šídák multiple comparison *post hoc* test, or a Mann–Whitney compare ranks test followed by Holm–Šídák multiple comparison *post hoc* test (e, g, i, k). When comparing control vs APAP viability and *de novo* DNA synthesis a two-tailed Student's unpaired *t*-test ($t = 0.8716$, df = 10 (b); $t = 10.76$, df = 9 (d); $t = 0.5543$, df = 8 (f); $t = 0.1872$, df = 8 (j)) or a one-sample two-tailed *t*-test (against control = 100, $t = 8.313$, df = 3 (h); $t = 12.04$, df = 3 (l)) were used. Data points are represented as mean±SEM. *$P < 0.05$; **$P < 0.01$; ***$P < 0.001$; ****$P < 0.0001$.

OXFORD
human reproduction
Human Reproduction, 2025, 1–1
https://doi.org/10.1093/humrep/deaf116
Supplementary Data

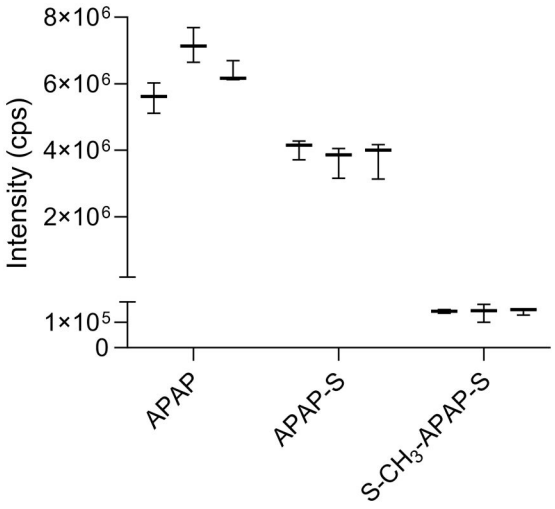

Supplementary Figure S4. Paracetamol (N-acetyl-para-aminophenol (APAP)) and two of its metabolites (APAP-S and S-CH_3-APAP-S) were detected in all exposure replicates. Median, minimum, maximum, and 25th and 75th percentiles of intensities of APAP, acetaminophen sulfate (APAP-S), and S-methyl-3-thioacetaminophen sulfate (S-CH_3-APAP-S) detected in biological replicates, with three technical media replicates, from cells exposed to APAP (n = 3). None of these compounds could be detected in the workup blanks and the DMSO controls (n = 3). Only 3 out of the 13 compounds from the suspect list usually detected *in vivo* could be detected with the highest confidence levels (i.e. with MS2 confirmation data).

OXFORD
human reproduction
Human Reproduction, 2025, 1–1
https://doi.org/10.1093/humrep/deaf116
Supplementary Data

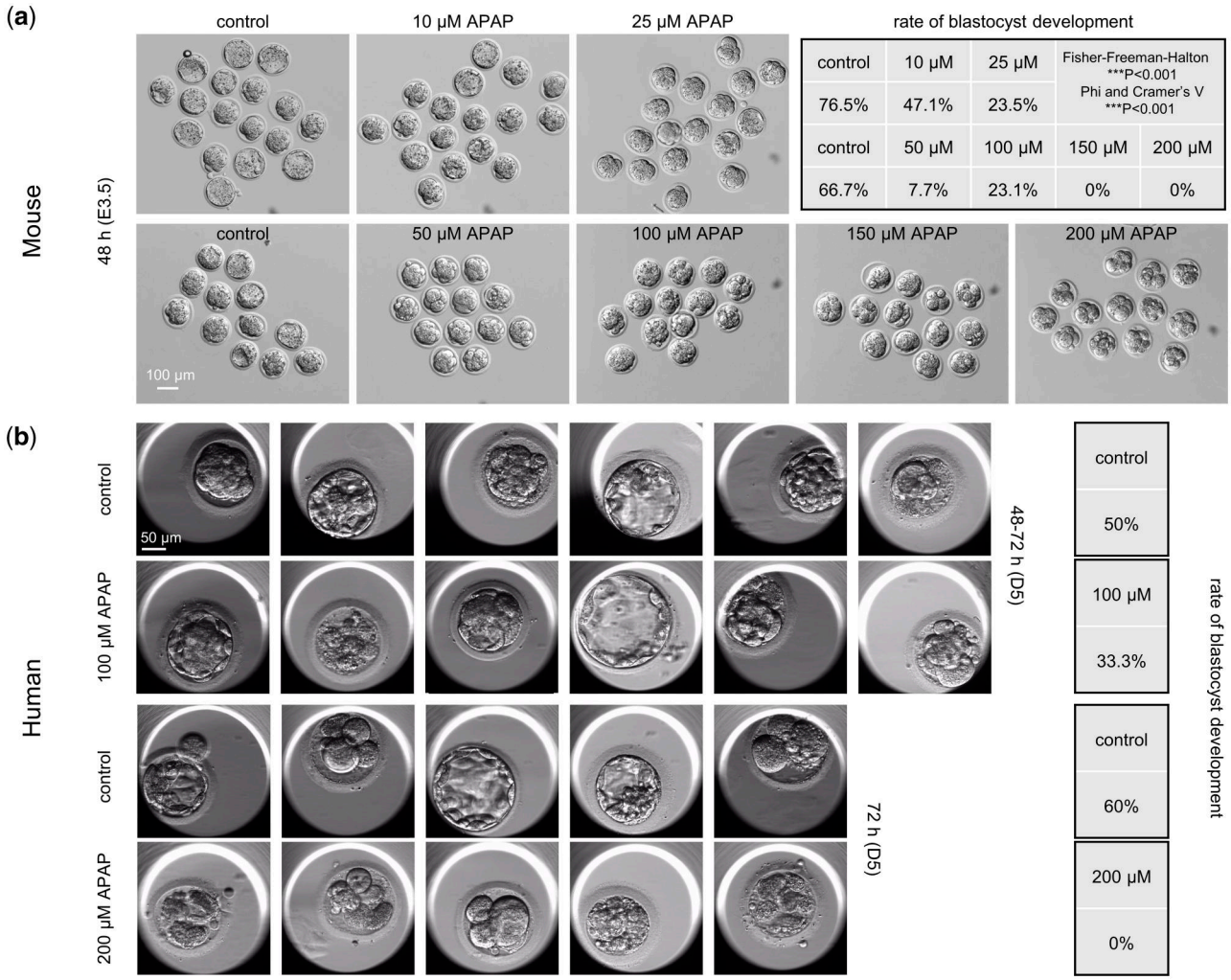

Supplementary Figure S5. Paracetamol (N-acetyl-para-aminophenol (APAP)) affects the blastocyst rate of mouse (C57BL/6JRj) and human embryos. (**a**) Light microscopy (LM) images of the mouse embryos cultured 48 h with media (control) or APAP at stated concentrations. Table displays the rate of blastocyst development at the given APAP concentrations and controls. To assess independence between the two variables embryo-to-blastocyst development and APAP concentration, a Fisher–Freeman–Halton exact test was performed with a significance of $P < 0.001$ and a Phi and Cramer's V strength association of 0.591, $P < 0.001$. (**b**) LM images of individual human embryos cultured 48–72 h in media (control) or media with APAP at stated concentrations. Tables display the rate of blastocyst-stage development at the given APAP concentrations and controls. The embryonic day in the parenthesis corresponds to their embryonic age at the end of the given exposure time.

OXFORD
human reproduction

Human Reproduction, 2025, 1–1
https://doi.org/10.1093/humrep/deaf116
Supplementary Data

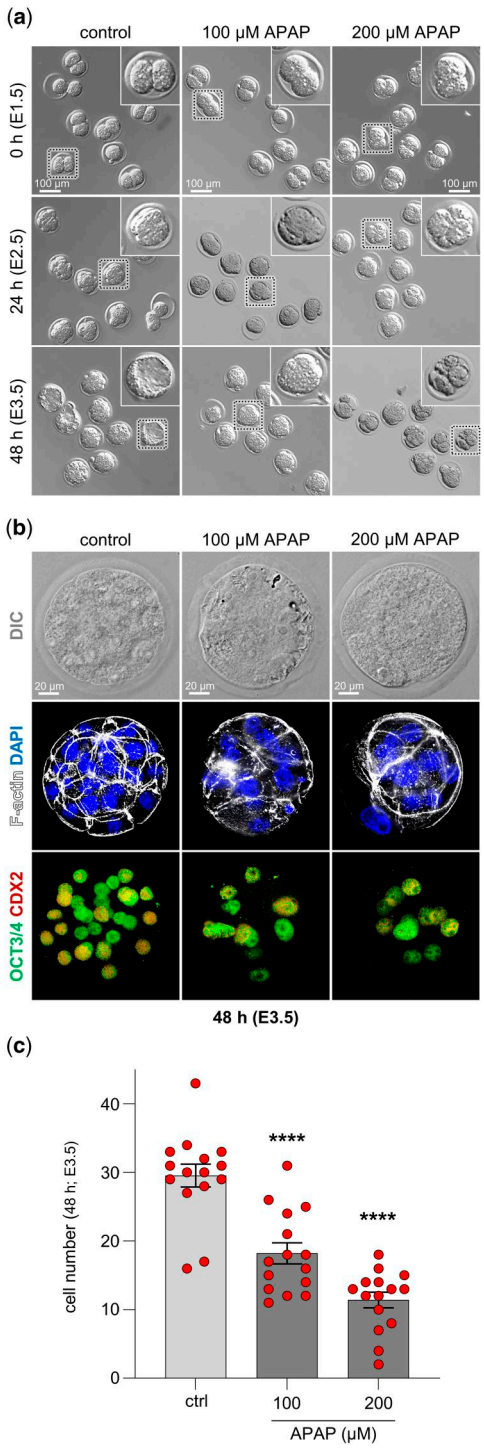

Supplementary Figure S6. Early pre-implantation development of outbred CD1 (RjOrl: SWISS) mouse embryos is disrupted by paracetamol (N-acetyl-para-aminophenol (APAP)) exposure. (**a**) Representative light microscopy images of developing embryos cultured for 0, 24, or 48 h in media (control) or media with APAP added at the stated concentrations. (**b**) Representative immunofluorescence microscopy (IFM) images of CD1 mouse embryos cultured for 48 h in control media or media with APAP at the stated concentrations. Upper panels: Differential interference contrast (DIC) images. Middle panels: F-actin stained by Phalloidin (white) and the nuclei stained using DAPI (blue). Lower panels: trophectoderm (TE) cells (red) stained by anti-CDX2 antibody and inner cell mass (ICM) cells stained by anti-OCT3/4 antibody (green). (**c**) Cell count quantification based on the IFM analysis of embryos cultured for 48 h in media (control; n = 15) or media with APAP at the stated concentrations (100 µM: n = 15, 200 µM: n = 15). The embryonic day in the parenthesis (e.g. E2.5) corresponds to their embryonic age at the end of the given exposure time. Statistical significance was tested with an ordinary one-way ANOVA analysis ($F(2, 42)=38.77$) followed by Holm–Šídák multiple comparison *post hoc* test (against control). Data points are represented as mean±SEM. ****$P < 0.0001$.

Supplementary Table S1. Metabolite annotation.

Name	Confid. level [1]	InChI	CAS	Formula	m/z Theoritical M-H	m/z Experimental M-H	m/z Δ ppm	Rt	MS/MS profiles (PASEF) Theoritical NEG	MS/MS profiles (PASEF) Experimental NEG
Parent										
Acetaminophen (APAP)	1	InChI=1S/C8H9NO2/c1-6(10)9-7-2-4-8(11)5-3-7/h2-5,11H,1H3,(H,9,10)	103-90-2	C8H9NO2	150,0561	150,0557	−2,3	4,7	107,0376	107,0372
Direct phase II reactions (Glu and S)										
Acetaminophen sulfate (APAP-S)	1	InChI=1S/C8H9NO5S/c1-6(10)9-7-2-4-8(5-3-7)14-15(11,12)13/h2-5H,1H3,(H,9,10)(H,11,12,13)	10066-90-7	C8H9NO5S	230,0129	230,0127	−0,9	4,5	79.9570, 107.0370, 150.0559	79.9570, 107.0374, 150.0556
Acetaminophen glucuronide (APAP-Glu)	n.d.	InChI=1S/C14H17NO8/c1-6(16)15-7-2-4-8(5-3-7)22-14-11(19)9(17)10(18)12(23-14)13(20)21/h2-5,9-12,14,17-19H,1H3,(H,15,16)(H,20,21)/t9-,10-,11+,12-,14+/m0/s1	16110-10-4	C14H17NO8	326,0881					
Catechol pathway (phase I+II)										
3-hydroxyacetaminophen (3-OH-APAP)	n.d.	InChI=1S/C8H9NO3/c1-5(10)9-6-2-3-7(11)8(12)4-6/h2-4,11-12H,1H3,(H,9,10)	37519-14-5	C8H9NO3	166,0510					
3-hydroxyacetaminophen sulfate (3-OH-APAP-S)	n.d.	InChI=1S/C8H9NO6S/c1-5(10)9-7-3-2-6(4-8(7)11)15-16(12,13)14/h2-4,11H,1H3,(H,9,10)(H,12,13,14)	53446-14-3	C8H9NO6S	246,0078					
3-methoxyacetaminophen glucuronide (3-OCH_3-APAP-Glu)	n.d.	InChI=1S/C15H19NO9/c1-6(17)16-7-3-4-8(9(5-7)23-2)24-15-12(20)10(18)11(19)13(25-15)14(21)22/h3-5,10-13,15,18-20H,1-2H3,(H,16,17)(H,21,22)/t10-,11-,12+,13-,15+/m0/s1	52092-55-4	C15H19NO9	356,0987					
Mercapturate pathway (phase I+II)										
3-(Cystein-S-yl) acetaminophen (APAP-Cys)	n.d.	InChI=1S/C11H14N2O4S/c1-6(14)13-7-2-3-9(15)10(4-7)18-5-8(12)11(16)17/h2-4,8,15H,5,12H2,1H3,(H,13,14)(H,16,17)/t8-/m0/s1	53446-10-9	C11H14N2O4S	269,0602					

(continued)

OXFORD
human reproduction
Human Reproduction, 2025, 1–2
https://doi.org/10.1093/humrep/deaf116
Supplementary Data

Supplementary Table S1. Continued

Name	Confid. level [1]	InChI	CAS	Formula	m/z			Rt	MS/MS profiles (PASEF)	
					Theoritical M-H	Experimental M-H	Δ ppm		Theoritical NEG	Experimental NEG
Acetaminophen mercapturate (NAC-APAP)	n.d.	InChI=1S/C13H16N2O5S/c1-7(16)14-9-3-4-11(18)12(5-9)21-6-10(13(19)20)15-8(2)17/h3-5,10,18H,6H2,1-2H3,(H,14,16)(H,15,17)(H,19,20)/t10-/m0/s1	52372-86-8	C13H16N2O5S	311,0707					
Thiomethyl shunt pathway										
3-thioacetaminophen glucuronide (SH-APAP-Glu)	n.d.		n.a.	C14H17NO8S	358,0602					
S-methyl-3-thioacetaminophen (S-CH_3-APAP)	n.d.	InChI=1S/C9H11NO2S/c1-6(11)10-7-3-4-8(12)9(5-7)13-2/h3-5,12H,1-2H3,(H,10,11)	37398-23-5	C9H11NO2S	196,0438					
S-methyl-3-thioacetaminophen sulfate (S-CH_3-APAP-S)	1	InChI=1S/C9H11NO5S2/c1-6(11)10-7-3-4-8(9(5-7)16-2)15-17(12,13)14/h3-5H,1-2H3,(H,10,11)(H,12,13,14)	78194-51-1	C9H11NO5S2	276,0006	276,0004	−0,7	5,8	79.9560, 138.0016, 165.9959, 181.0204, 196.0437	79.9570, 138.0017, 165.996, 181.0206, 196.0436
S-methyl-3-thioacetaminophen glucuronide (S-CH_3-APAP-Glu)	n.d.	InChI=1S/C15H19NO8S/c1-6(17)16-7-3-4-8(9(5-7)25-2)23-15-12(20)10(18)11(19)13(24-15)14(21)22/h3-5,10-13,15,18-20H,1-2H3,(H,16,17)(H,21,22)/t10-,11-,12+,13-,15+/m0/s1	78180-86-6	C15H19NO8S	372,0759					
S-methyl-3-thioacetaminophen sulphoxide sulfate (SO-CH_3-APAP-S)	n.d.		n.a.	C9H11NO6S2	291,9955					
S-methyl-3-thioacetaminophen sulphoxide glucuronide (SO-CH_3-APAP-Glu)	n.d.		n.a.	C15H19NO9S	388,0708					

[1] Confidence level according to Schymanski, E. L. *et al.* Environ Sci Technol 48, 2097-2098, doi: 10.1021/es5002105 (2014). 1 = confirmed structure: confirmation via appropriate measurement of a reference standard with MS, MS/MS, and retention time matching. InChI, IUPAC International Chemical Identifier; CAS: Chemical Abstracts Service; m/z, mass to charge ratio of molecular ion as M + H or M−H adducts in positive and negative modes, respectively; MS/MS, fragmentation profiles generated using the Parallel Accumulation Serial Fragmentation (PASEF) injection mode in negative; NEG, negative mode; n.d., not detected; n.a., not applicable.

Supplementary Table S2. Overview of the human blastocyst-stage embryos before, during, and after 6 h of control exposure.

Exposure	Blastocyst info		Gardner score[1]					IFM analysis of ICM		
Control #	Donor age	Day of freeze	Pre-freeze	Post-warming	0 h exposure	3 h exposure	6 h exposure	# OCT3/4 positive cells	# EdU positive cells	%
1	24	5	4AB	4AB	4AB	5BB	5AB	18	13	72,2
2	24	5	3BB	3BB	3BB	4BB	4BB	17	11	64,7
3	24	5	4BA	4BA	minor collapse	5AA	5BA	16	13	81,3
4	24	5	4BB	4BB	4BB	4BB	3BA	16	12	75,0
5	39	5	1BB	1BB	1	1	2	n/a	n/a	n/a
6	39	5	4AA	4AA	4, 50% atresia	4, 50% atresia	4AB, 25% atresia, fully expanded	12	10	83,3
7	30	6	4BB	4BB	4BB	4BB	4BA	3	2	66,7
8	39	5	4BB	4BB	4BA	5BA	4AA	11	9	81,8
9	30	6	4BA	4BA	4, 75% atresia	4, 25% atresia	4BB, 25% atresia	3	2	66,7
10	36	5	4AA	4AA	4AA	5BA	5AA	22	17	77,3
11	36	5	4AA	4AB	4, 75% atresia	4, 75% atresia	4AC, 75% atresia	16	12	75,0
12	23	5	4BB	4BB	5BB, 25% atresia	5BB	4BB	11	8	72,7
13	34	6	4AA	4AA	4BA	5BA	5BA	5	3	60,0
14	23	5	4AA	4AA	4, partially expanded	6 CB, minus zona	collapse	n/a	n/a	n/a
15	27	5	4AA	4AA	4, minor collapse, 25% atresia	4BB, partially expanded	4BB, 25% atresia	n/a	n/a	n/a
16	25	5	5AA	5AA	5, partially expanded	4AA	5AB	n/a	n/a	n/a
17	42	5	2	3BB	3BB	4AB	4AA, partially collapse	16	10	62,5
18	35	6	5BA	4AA	4AA	4CA	4CA	6	3	50,0
19	32	5	4BB	3BB	3BB	4AA	4AB	10	3	30,0
20	40	5	4AA	4AB	4AB	4AB	4BB	12	7	58,3
21	31	5	4AA	5AA	5AA	5AA	5AA	18	12	66,7
22	31	5	4BA	4, collapse	4, collapse	4BB	4AA	12	7	58,3
23	19	5	2BB	2BB	2BB	3BB	4BB	10	8	80,0
24	34	5	4BB	collapse	collapse	4AA	4BB	14	12	85,7
25	34	5	4AA	4AA	4AA	5BA	5BA	12	7	58,3
26	34	6	5BA	partially collapse, 25% atresia	partially collapse, 25% atresia	4BB	4BB, 25% atresia	7	6	85,7
27	42	5	4AB	partially collapse	partially collapse	3AB	4AB	23	17	73,9
28	31	6	4AB	partially collapse	partially collapse	partially collapse	partially collapse	6	3	50,0
29	35	6	4BA	3BB	3BB	4BA	collapse	8	5	62,5
30	28	6	4BB	5AA	5AA	4AA	4AA	12	6	50,0
31	33	5	4AA	collapse	collapse	partially expanded	4BB	11	6	54,5
32	21	6	4BB	4AA	4AA	5BA	5BA	6	3	50,0
33	41	5	2AB	2	2	3AB	4AB	7	4	57,1
34	41	5	3AA	partially collapse	partially collapse	4AA	4AA	5	2	40,0

[1] Graded according to Gardner, D K *et al.* 'Blastocyst score affects implantation and pregnancy outcome: toward a single blastocyst transfer.' Fertility and sterility vol. 73,6 (2000): 1155–8. doi: 10.1016/s0015-0282(00)00518-5.

Gardner scoring not performed if trophectoderm (TE) and/or inner cell mass (ICM) were not identifiable; n/a, not available, due to an indefinable ICM or loss during the whole-mount immunofluorescence staining procedure; IFM, immunofluorescence microscopy.

OXFORD
human reproduction
Human Reproduction, 2025, 1–1
https://doi.org/10.1093/humrep/deaf116
Supplementary Data

Supplementary Table S3. Overview of the human blastocyst-stage embryos before, during, and after 6 h of APAP exposure.

Exposure		Blastocyst info		Gardner score[1]					IFM analysis of ICM		
APAP #	Concentration (μM)	Donor age	Day of freeze	Pre-freeze	Post-warming	0 h exposure	3 h exposure	6 h exposure	# OCT3/4 positive cells	# EdU positive cells	%
101	200	24	5	4AB	4AB	4AB	5BA	5AA	17	5	29,4
102	200	24	5	3AA	3AA	3AA	4BA	5BA	10	4	40,0
103	200	24	5	4AB	4AB	minor collapse	5BB	5BB	n/a	n/a	n/a
104	200	24	5	4BB	5AB minor collapse	minor collapse	5AB	4, collapse	7	1	14,3
105	200	39	5	1BA	1BA	1BA	2	3BA	n/a	n/a	n/a
106	200	39	5	4AA	5BB	4, 50% atresia	5BB, 25% atresia	5BA	12	5	41,7
107	200	32	6	4BB	4BB minor collapse	4BB	5BC	4BB, 25% atresia	n/a	n/a	n/a
108	200	41	5	4AA	4AA	4AA, almost expanded	4AB	5AA	5	4	80,0
109	200	32	6	4BB	4BB minor collapse	50% atresia, partially expanded	4, 50% atresia	4BB, 50% atresia	6	2	33,3
110	200	36	5	3BB	3BB	3BB	4BA	5BA	n/a	n/a	n/a
111	200	36	5	3BB	3BB minor collapse	3, 50% atresia	3, 25% atresia	3BB, 25% atresia	n/a	n/a	n/a
112	200	23	5	4BB	4BB	4BB	4, partially collapse	4BB	8	8	100,0
113	200	34	6	4AB	4AB	4, 50% atresia	4BB	4BA	7	3	42,9
114	200	23	5	4AA	4AA	4BB	4BA	5BB	8	6	75,0
115	200	27	5	4AA	4AA	4, partially expanded	4AA	6BA	n/a	n/a	n/a
116	200	25	5	4AB	4AB	4, collapse	4	4BB, 25% atresia	n/a	n/a	n/a
117	100	42	5	2	2	2	2	3BC	n/a	n/a	n/a
118	100	35	6	5BB	3BB	3BB	4BB	4BB	9	3	33,3
119	100	32	6	4AA	4BA	4BA	4AB, minor collapse	4BA, minor collapse	8	5	62,5
120	100	40	5	5AA	5AA	5AA	4AA	4BA	11	6	54,5
121	100	31	5	4BA	4BA	4BA	4BA, minor collapse	5BA	15	6	40,0
122	100	31	5	5AA	4, partially collapse	4, partially collapse	4, partially collapse	5BA	n/a	n/a	n/a
123	100	19	5	2BB	collapse	collapse	partially collapse	2??	n/a	n/a	n/a
124	100	34	5	4BB	4BB	4BB	4BB	4BB	20	11	55,0
125	100	34	5	4AA	4, partially collapse	4, partially collapse	4AA	4AA	14	12	85,7
126	100	34	6	5AA	partially collapse	partially collapse	partially collapse	5BA	n/a	n/a	n/a
127	100	37	5	4AA	collapse	collapse	3BA	4AB	9	2	22,2
128	100	28	6	5BB	collapse	collapse	4, 75% atresia	5CC	n/a	n/a	n/a
129	100	27	6	4BB	4AA	4AA	4BB	4BB, partially expanded	2	0	0,0
130	100	28	6	4BB	3BB	3BB	4BB	5BB	n/a	n/a	n/a
131	100	33	5	3AB	collapse	collapse	3AB	4AA	4	2	50,0
132	100	22	5	3BB	collapse	collapse	3BC	4BB	10	6	60,0
133	100	41	5	2AA	2	2	4AB	4AA	14	11	78,6
134	100	41	5	5AA	collapse	collapse	collapse	3CC, partially expanded	n/a	n/a	n/a

[1] Graded according to Gardner, D K *et al.* 'Blastocyst score affects implantation and pregnancy outcome: toward a single blastocyst transfer.' Fertility and sterility vol. 73,6 (2000): 1155–8. doi: 10.1016/s0015-0282(00)00518-5.

Gardner scoring not performed if trophectoderm (TE) and/or inner cell mass (ICM) were not identifiable; n/a, not available, due to an indefinable ICM or loss during the whole-mount immunofluorescence staining procedure; IFM, immunofluorescence microscopy; APAP, paracetamol.

OXFORD
human reproduction
Human Reproduction, 2025, 1–1
https://doi.org/10.1093/humrep/deaf116
Supplementary Data

OXFORD

human reproduction

Human Reproduction, 2025, 1–1

https://doi.org/10.1093/humrep/deaf116

Supplementary Data

Supplementary Table S4. Raw flow cytometry cell cycle data for HEK293, HuES4, and H1 cell lines.

HEK293

Control	#1 Events	%	#2 Events	%	#3 Events	%	#4 Events	%	#5 Events	%	#6 Events	%	Mean %
G0/G1	6109	58.37	6212	61.05	6145	59.92	6402	60.91	6466	61.53	6310	59.87	60.28
S	912	8.71	895	8.80	958	9.34	1023	9.73	904	8.60	1005	9.54	9.13
G2/M	3445	32.92	3068	30.15	3139	30.61	3086	29.36	3139	29.87	3224	30.59	30.59
APAP	#1 Events	%	#2 Events	%	#3 Events	%	#4 Events	%	#5 Events	%	#6 Events	%	Mean %
G0/G1	6066	59.84	5756	55.25	6081	59.45	5901	56.76	5907	56.74	6019	57,76	57.63
S	1340	13.22	1296	12.44	1277	12.49	1448	13.93	1486	14.27	1381	13.25	13.27
G2/M	2731	26.94	3367	32.32	2869	28.05	3048	29.32	3017	28.98	3020	28,98	29.10

HuES4

Control	#1 Events	%	#2 Events	%	#3 Events	%	#4 Events	%	#5 Events	%	Mean %
G0/G1	3086	31.59	3864	36.54	3775	36.73	3077	37.65	3564	33.46	35.19
S	592	6.06	1387	13.11	515	5.01	184	2.25	579	5.44	6.37
G2/M	6091	62.35	5325	50.35	5989	58.26	4911	60.10	6508	61.10	58.43
APAP	#1 Events	%	#2 Events	%	#3 Events	%	#4 Events	%	#5 Events	%	Mean %
G0/G1	3425	34.54	3831	37.24	3963	36.17	2919	41.02	3700	34.03	36.60
S	1099	11.08	1786	17.36	767	7.00	351	4.93	831	7.64	9.60
G2/M	5391	54.37	4671	45.40	6228	56.84	3846	54.05	6342	58.33	53.80

H1

Control	#1 Events	%	#2 Events	%	#3 Events	%	#4 Events	%	#5 Events	%	Mean %
G0/G1	3545	35.66	3898	38.24	4267	39.39	4790	45.84	4082	38.79	39.58
S	640	6.44	741	7.27	714	6.59	328	3.14	766	7.28	6.14
G2/M	5756	57.90	5554	54.49	5851	54.02	5332	51.02	5676	53.93	54.27
APAP	#1 Events	%	#2 Events	%	#3 Events	%	#4 Events	%	#5 Events	%	Mean %
G0/G1	4011	40.19	3743	37.22	4653	42.07	3796	47.36	4216	40.01	41.37
S	760	7.62	1106	11.00	1147	10.37	426	5.32	852	8.09	8.48
G2/M	5209	52.19	5208	51.78	5260	47.56	3793	47.32	5470	51.91	50.15

APAP, paracetamol.